*Journal of Sound and Vibration* (2001) **241**(4), 605–633
doi:10.1006/jsvi.2000.3313, available online at http://www.idealibrary.com on IDEAL®

# FREE-VIBRATION ANALYSIS OF PLATES AND SHELLS WITH A NINE-NODE ASSUMED NATURAL DEGENERATED SHELL ELEMENT

S. J. Lee

*Integrated Safety Assessment Team, Korea Atomic Energy Research Institute, P.O. Box* 105, *Yusung, Taejon* 305-600, *South Korea, E-mail: sjlee@kaeri.re.kr*

AND

S. E. Han

*Department of Architectural Engineering, Inha University, Inchon* 402-751, *South Korea*

(*Received* 7 *December* 1998, *and in final form* 20 *July* 2000)

A study on the free-vibration analysis of plates and shells is described in this paper. In order to determine the natural frequencies of plates and shells, a nine-node degenerated shell element is developed by using the degenerated solid concept based on Reissner–Mindlin (RM) assumptions which allow the shear deformation and rotatory effect to be considered. All terms required in the shell finite element (FE) formulation are defined in the natural domain. In particular, assumed natural strains are derived to alleviate the locking phenomena inherited in the RM shell elements. The natural constitutive equation is used in conjunction with the natural strain terms. The proposed shell FE formulation offers significant implementation advantages since it consistently uses the natural co-ordinate system. Various numerical examples are carried out and its results are then compared with the existing exact solutions and the numerical solutions calculated by other shell FEs.


## 1. INTRODUCTION

In Engineering practice, it is often of vital importance to conduct a free-vibration analysis of structures and to use the resulting information in the design process so that the resonant behaviour of the structures can be prevented for the given loading conditions.

The vibration of thin shells was discussed in the early work of Love [1]. Since then many researchers have dealt with shell vibration using classical thin-shell theory. In particular, Donnell [2] used classical thin shallow-shell theory to understand the free-vibration behaviour of shells and subsequent research has been reviewed by Leissa [3], Qatu [4] and Liew *et al.* [5]. However, until the 1960s shell vibration research focused on individual types of shell and the applications of shell theory were limited to specific geometries.

In order to investigate the vibration behaviour of complex shell structures, the FE method was inevitably introduced and it has subsequently become the most popular method. In particular, many shallow shell elements have been developed since the early work of Adini [6]. As noted by Gallagher [7], the development of thin-shell FEs began with application to aerospace vehicles. During the early 1960s, a large number of thin-shell elements were therefore developed to meet the demands of the aerospace industry. In this period, three-dimensional elements were also widely used to design thick-walled shell stuctures.

0022-460X/01/140605 + 29 $35.00/0 

However, an innovative approach, the so-called degenerated solid concept, was introduced by Ahmad *et al.* [8]. Nowadays, the degenerated shell element based on this concept is one of the most popular shell FE formulations. Generally, RM assumptions have been adopted in the development of such elements and therefore the mass matrix includes rotatory inertia effects. It has been shown that the accuracy of the frequency is improved by the rotatory inertia terms in the mass matrix for thick shells as well as the inclusion of transverse shear effects in the stiffness matrix. However, it is found that there are serious defects such as locking phenomena in the degenerated shell element.

As an early remedy to locking phenomena inherited in the degenerated shell element based on RM assumptions, the so-called reduced integration [9, 10] was used in the transverse shear energy term. However, the shell elements with the reduced integration suffered from the mechanism and later other methods, such as assumed strain methods [11] and stabilization method [12], have been proposed by many researchers. The assumed strain methods have been successfully used in stress FE analysis. However, in contrast, there are few investigations on the performance of the assumed natural strain shell element in the shell free-vibration analysis.

In this paper, therefore, the natural domain-based shell formulation is provided with emphasis on the terms related to the stiffness and mass matrices. Then a set of bench-marks are presented to show the application of the shell formulation to various types of shells under free-vibration conditions.

Although a new shell element has been developed by means of calculating the natural frequencies of shells, it is important to evaluate the performance of shell FE in the plate situations, which may be considered as a special form of shells with no curvature. Recent work on the free-vibration analysis of plate element can be found in open literature. In particular, the plate vibration problems can be consulted in reference [13].

Note that the Lobatto integration rule [14] is adopted to evaluate the mass matrix and the subspace iteration method [15, 16] is employed in the calculation of the lowest eigenvalues of shells. It should be noted that Gauss integration rule is used in the first example to provide some comparative results with the Lobatto integration rule.

## 2. GEOMETRY AND KINEMATICS OF SHELLS

The geometry of degenerated shell element is represented by two vectors ($\mathbf{x}^a_{top}$ and $\mathbf{x}^a_{bot}$), which are the position vectors of the original solid element as shown in Figure 1. The degeneration of the solid element requires the use of the vector $\hat{\mathbf{v}}^a_3$ which allows the top and bottom nodes to be degenerated into the node at the shell mid-surface. The definition of the shell geometry [8] can be written as

$$\mathbf{x}(\xi_1, \xi_2, \xi_3) = \sum_{a=1}^{9} N_a(\xi_1, \xi_2) \left[ \bar{\mathbf{x}}^a + \frac{\xi_3 h^a}{2} \hat{\mathbf{v}}^a_3 \right], \tag{1}$$

where $\mathbf{x}$ is the position vector of a generic point in the element domain, $\bar{\mathbf{x}}^a = \frac{1}{2}(\mathbf{x}^a_{top} + \mathbf{x}^a_{bot})$ denotes the position vector of node $a$ in the mid-surface, $h^a$ is the thickness of the shell at node $a$ and $\hat{\mathbf{v}}^a_3$ is the unit vector through thickness direction at node $a$ which is created using

$$\hat{\mathbf{v}}^a_3 = \frac{\mathbf{x}^a_{top} - \mathbf{x}^a_{bot}}{|\mathbf{x}^a_{top} - \mathbf{x}^a_{bot}|} \tag{2}$$

in which $\mathbf{x}^a_{top}$ denotes the position vector of node $a$ in the top surface and $\mathbf{x}^a_{bot}$ denotes the position vector of node $a$ in the bottom surface as shown in Figure 1.

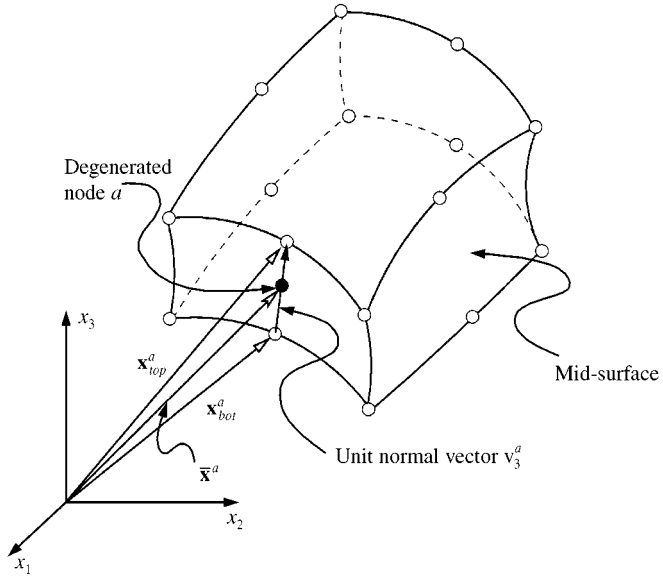


Figure 1. Degenerated solid concept illustrated by using a solid element.

However, it should be noted that the shell normal can be created by using the co-ordinates of the shell mid-surface. In most cases, the third axis of the local co-ordinate system [17] is used as the shell normal at the nodal point. Therefore, the above equation can be replaced by the following form:

$$\mathbf{x}(\xi_1, \xi_2, \xi_3) = \sum_{a=1}^{9} N_a(\xi_1, \xi_2) \left[ \bar{\mathbf{x}}^a + \frac{\xi_3 h^a}{2} \hat{\mathbf{d}}^a \right] \tag{3}$$

in which $\hat{\mathbf{d}}^a$ is established at node $a$ by using

$$\hat{\mathbf{d}}^a(\xi_1, \xi_2) = \frac{\bar{\mathbf{x}}^a_{,\xi_1}(\xi_1, \xi_2) \times \bar{\mathbf{x}}^a_{,\xi_2}(\xi_1, \xi_2)}{|\bar{\mathbf{x}}^a_{,\xi_1}(\xi_1, \xi_2) \times \bar{\mathbf{x}}^a_{,\xi_2}(\xi_1, \xi_2)|}. \tag{4}$$

Note that the vector $\hat{\mathbf{d}}^a$ can be replaced with $\hat{\mathbf{v}}^a_3$ if the co-ordinates of top and bottom shell surface are available.

The displacement field $\mathbf{u}$ used in the present shell element having six degrees of freedom per node can be defined as

$$\mathbf{u}(\xi_1, \xi_2, \xi_3) = \sum_{a=1}^{9} N_a(\xi_1, \xi_2) \left[ \bar{\mathbf{u}}^a + \frac{\xi_3 h^a}{2} (\mathbf{R}^a_s - \mathbf{I}_{3\times 3}) \hat{\mathbf{d}}^a \right], \tag{5}$$

where the unit normal vector at node $a$, namely $\hat{\mathbf{d}}^a$, is defined using equation (4), $\mathbf{I}$ is the identity matrix and the rotational matrix $\mathbf{R}^a_s$ has the form

$$\mathbf{R}^a_s = \begin{bmatrix} 1 & -\theta^a_3 & \theta^a_2 \\ \theta^a_3 & 1 & -\theta^a_1 \\ -\theta^a_2 & \theta^a_1 & 1 \end{bmatrix} \tag{6}$$

in which $\theta^a_i$ denotes the rotations associated with the components of the shell normal $\hat{\mathbf{d}}^a$.

For later use, the displacement field in equation (5) can be written in the following form:

$$\mathbf{u} = \sum_{a=1}^{9} \mathbf{N}_a \mathbf{u}^a, \tag{7}$$

where $\mathbf{u}^a$ is the displacement vector at the node $a$ and the shape function matrix $\mathbf{N}_a$ associated with the node $a$ is

$$\mathbf{N}_a = N_a \begin{bmatrix} 1 & 0 & 0 & 0 & h_s^a(\xi_3)\hat{d}_z^a & -h_s^a(\xi_3)\hat{d}_y^a \\ 0 & 1 & 0 & -h_s^a(\xi_3)\hat{d}_z^a & 0 & h_s^a(\xi_3)\hat{d}_x^a \\ 0 & 0 & 1 & h_s^a(\xi_3)\hat{d}_y^a & -h_s^a(\xi_3)\hat{d}_x^a & 0 \end{bmatrix} \tag{8}$$

in which $h_s^a(\xi_3) = \xi_3 h^a/2$ and $\hat{d}_x^a$, $\hat{d}_y^a$ and $\hat{d}_z^a$ are the components of the unit normal vector $\hat{\mathbf{d}}^a$ in the global co-ordinate system.

## 3. SHELL FORMULATIONS

All terms used in the derivation of the present shell element are expressed in terms of the natural co-ordinates. Therefore the natural strains and the constitute equation are used.

### 3.1. STRAIN DEFINITION

The linear terms of natural strains can be derived from the natural Lagrangian strains [18]

$$\tilde{\varepsilon}_{ij} = \frac{1}{2}\left(\frac{\partial u_k}{\partial \xi_i}\frac{\partial x_k}{\partial \xi_j} + \frac{\partial u_k}{\partial \xi_j}\frac{\partial x_k}{\partial \xi_i}\right). \tag{9}$$

In the discretized FE domain, the natural strain–displacement matrix $\tilde{\mathbf{B}}^a$ can be obtained by using the following operation:

$$\tilde{\mathbf{B}}^a = \mathbf{L}[\tilde{\boldsymbol{\varepsilon}}_p, \tilde{\boldsymbol{\varepsilon}}_s] \tag{10}$$

in which $\tilde{\boldsymbol{\varepsilon}}_p = [\varepsilon_{11}, \varepsilon_{22}, \varepsilon_{12}]^{\mathrm{T}}$ is the in-plane strain term and $\tilde{\boldsymbol{\varepsilon}}_s = [\varepsilon_{13}, \varepsilon_{23}]^{\mathrm{T}}$ is the transverse shear strain term and the partial differential operator $\mathbf{L}$ is

$$\mathbf{L}^{\mathrm{T}} = \{\partial/\partial u_1^a, \partial/\partial u_2^a, \partial/\partial u_3^a, \partial/\partial \theta_1^a, \partial/\partial \theta_2^a, \partial/\partial \theta_3^a\}. \tag{11}$$

Because of the locking phenomena inherited in the degenerated RM shell element, the standard strain–displacement matrix $\tilde{\mathbf{B}}^a$ is substituted with assumed natural strains in this study. The sampling points used in the formulation of assumed natural strains are presented in Figure 2. The interpolation functions used in formulating the assumed strains are based on Lagrangian interpolation polynomials as proposed by Huang and Hinton [19]. Consequently, the substitute assumed that natural strains $\tilde{\varepsilon}^A$ can be defined in the following form:

$$\tilde{\varepsilon}_{11}^A = \sum_{i=1}^{2}\sum_{j=1}^{3} \mathscr{P}_i(\xi_1)\mathscr{Q}_j(\xi_2)\tilde{\varepsilon}_{11}^{\delta}, \qquad \tilde{\varepsilon}_{22}^A = \sum_{i=1}^{2}\sum_{j=1}^{3} \mathscr{P}_i(\xi_2)\mathscr{Q}_j(\xi_1)\tilde{\varepsilon}_{22}^{\delta},$$

$$\tilde{\varepsilon}_{12}^A = \sum_{i=1}^{2}\sum_{j=1}^{2} \mathscr{P}_i(\xi_1)\mathscr{P}_j(\xi_2)\tilde{\varepsilon}_{12}^{\delta}, \tag{12}$$

$$\tilde{\varepsilon}_{13}^A = \sum_{i=1}^{2}\sum_{j=1}^{3} \mathscr{P}_i(\xi_1)\mathscr{Q}_j(\xi_2)\tilde{\varepsilon}_{13}^{\delta}, \qquad \tilde{\varepsilon}_{23}^A = \sum_{i=1}^{2}\sum_{j=1}^{3} \mathscr{P}_i(\xi_2)\mathscr{Q}_j(\xi_1)\tilde{\varepsilon}_{23}^{\delta}$$

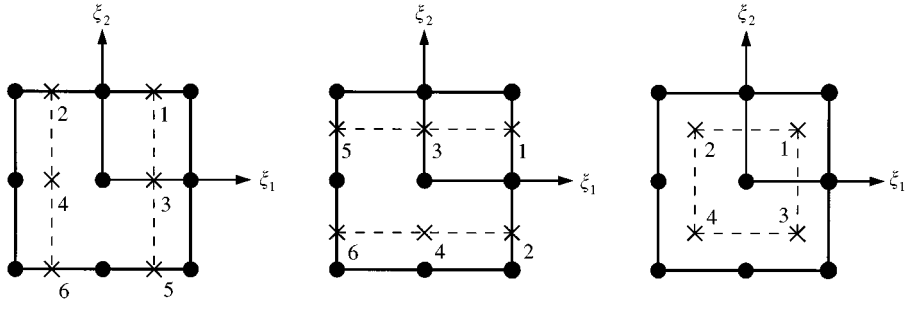


Figure 2. The sampling point for the natural assumed strains; left for $\tilde{\varepsilon}_{11}$, $\tilde{\varepsilon}_{13}$ centre for $\tilde{\varepsilon}_{22}$, $\tilde{\varepsilon}_{23}$ and right for $\tilde{\varepsilon}_{12}$.

in which $\delta = 2(j-1) + i$ denotes the position of the sampling point as shown in Figure 2 and the shape functions $\mathscr{P}_i(\xi)$ and $\mathscr{Q}_i(\xi)$ are

$$\mathscr{P}_1(\xi) = \tfrac{1}{2}(1 + \sqrt{3}\xi), \qquad \mathscr{P}_2(\xi) = \tfrac{1}{2}(1 - \sqrt{3}\xi),$$
$$\mathscr{Q}_1(\xi) = \tfrac{1}{2}\xi(\xi + 1), \qquad \mathscr{Q}_2(\xi) = 1 - \xi^2, \qquad \mathscr{Q}_3(\xi) = \tfrac{1}{2}\xi(\xi - 1). \tag{13}$$

The assumed natural strains $\tilde{\varepsilon}^A$ derived from equation (12) are used in the present shell element instead of the strains $\tilde{\varepsilon}$ of equation (9) obtained from the displacement field.

### 3.2. CONSTITUTIVE EQUATION

The stress tensor for elastically isotropic materials can be written as

$$\sigma_{ij} = D_{ijkl}\varepsilon_{kl} = [\lambda\delta_{ij}\delta_{kl} + \mu(\delta_{ik}\delta_{jl} + \delta_{il}\delta_{jk})]\,\varepsilon_{kl}, \tag{14}$$

where $\sigma_{ij}$ is the Cauchy stress, $D_{ijkl}$ are a fourth order isotropic material tensor and $\varepsilon_{kl}$ is the small strains. $\lambda$ and $\mu$ are the Lame constant and $\delta_{ij}$ is the Kronecka delta.

An isotropic material is not direction dependent. However, a scaling factor has to be introduced when elastic constants are formed in the natural co-ordinate domain. The natural stress tensor can be written as follows:

$$\tilde{\sigma}_{\alpha 3} = \tilde{D}_{\alpha\beta\gamma\delta}\tilde{\varepsilon}_{\gamma\delta} = \tilde{J}_o[\lambda g_{\alpha\beta}g_{\gamma\delta} + \mu(g_{\alpha\gamma}g_{\beta\delta} + g_{\alpha\delta}g_{\beta\gamma})]\tilde{\varepsilon}_{\gamma\delta}, \tag{15}$$

where the natural constitutive tensor is obtained from

$$\tilde{D}_{\alpha\beta\gamma\delta} = \tilde{J}_o \frac{\partial\xi_\alpha}{\partial x_i}\frac{\partial\xi_\beta}{\partial x_j}\frac{\partial\xi_\gamma}{\partial x_k}\frac{\partial\xi_\delta}{\partial x_l} D_{ijkl} \tag{16}$$

and $\tilde{J}_o = \det[\partial x_i/\partial\xi_\alpha]$ and $g_{\alpha\beta} = \partial\xi_\alpha/\partial x_i \partial\xi_\beta/\partial x_i$.

The above equation can be reduced using the generalized plane stress condition $\tilde{\sigma}_3 = 0$ with the assumption that the effect of variation of natural constitutive parameters in the thickness direction can be neglected as follows:

$$\bar{D}_{\alpha\beta\gamma\delta} = \bar{J}_o[\bar{\lambda}\bar{g}_{\alpha\beta}g_{\gamma\delta} + \mu(\bar{g}_{\alpha\gamma}\bar{g}_{\beta\delta} + \bar{g}_{\alpha\delta}\bar{g}_{\beta\gamma})], \tag{17}$$

where $\bar{\lambda}$ is the reduced Lamé's constant for the generalized plane stress–strain relationship, $\bar{J}_o$ and $\bar{g}_{\alpha\beta}$ are calculated using $\tilde{J}_o$ and $g_{\alpha\beta}$ at $\xi_3 = 0$.

Now the natural stresses can be rewritten in matrix form

$$\begin{Bmatrix} \tilde{\boldsymbol{\sigma}}_p \\ \tilde{\boldsymbol{\sigma}}_s \end{Bmatrix} = \begin{bmatrix} \tilde{\mathbf{D}}_p^* & 0 \\ 0 & \tilde{\mathbf{D}}_s^* \end{bmatrix} \begin{Bmatrix} \tilde{\varepsilon}_p \\ \tilde{\varepsilon}_s \end{Bmatrix}, \tag{18}$$

where $\tilde{\boldsymbol{\sigma}}_p = [\tilde{\sigma}_{11}, \tilde{\sigma}_{22}, \tilde{\sigma}_{12}]^{\mathrm{T}}$ is in-plane stress term and $\tilde{\boldsymbol{\sigma}}_s = [\tilde{\sigma}_{13}, \tilde{\sigma}_{23}]^{\mathrm{T}}$ is the transverse shear stress term and the natural in-plane and transverse shear rigidity matrices $\tilde{\mathbf{D}}_p^*, \tilde{\mathbf{D}}_s^*$ are

$$\tilde{\mathbf{D}}_p^* = \bar{J}_o \begin{bmatrix} \alpha \bar{\mathrm{g}}_{11}^2 & \beta \bar{\mathrm{g}}_{11}\bar{\mathrm{g}}_{22} + 2\bar{\mathrm{g}}_{12}^2 & \alpha \bar{\mathrm{g}}_{11}\bar{\mathrm{g}}_{12} \\ \beta \bar{\mathrm{g}}_{11}\bar{\mathrm{g}}_{22} + 2\bar{\mathrm{g}}_{12}^2 & \alpha \bar{\mathrm{g}}_{22}^2 & \alpha \bar{\mathrm{g}}_{12}\bar{\mathrm{g}}_{22} \\ \alpha \bar{\mathrm{g}}_{11}\bar{\mathrm{g}}_{12} & \alpha \bar{\mathrm{g}}_{12}\bar{\mathrm{g}}_{22} & \beta \bar{\mathrm{g}}_{12}^2 + \mu(\bar{\mathrm{g}}_{11}\bar{\mathrm{g}}_{22} + \bar{\mathrm{g}}_{12}^2 \end{bmatrix},$$

$$\tilde{\mathbf{D}}_s^* = \bar{J}_o \begin{bmatrix} k_s\mu\, \bar{\mathrm{g}}_{11}\bar{\mathrm{g}}_{33} & k_s\mu\, \bar{\mathrm{g}}_{12}\bar{\mathrm{g}}_{33} \\ k_s\mu\, \bar{\mathrm{g}}_{12}\bar{\mathrm{g}}_{33} & k_s\mu\, \bar{\mathrm{g}}_{22}\bar{\mathrm{g}}_{33} \end{bmatrix} \tag{19}$$

in which the parameters $\alpha$ and $\beta$ are

$$\alpha = \frac{4\mu(\lambda + \mu)}{\lambda + 2\mu} = \frac{E}{1 - \nu^2} \quad \text{and} \quad \beta = \frac{2\mu\lambda}{\lambda + 2\mu} = \frac{\nu E}{1 - \nu^2} \tag{20}$$

and $k_s$ is the shear correction factor which is taken as $\frac{5}{6}$ for an isotropic material and $\nu$ is the Poisson ratio.

### 3.3. EQUILIBRIUM EQUATION

In the absence of external loads and damping effects, the dynamic equilibrium equation based on the principle of virtual work (or more precisely virtual power) can be written as

$$\int_\Omega [\delta\boldsymbol{\varepsilon}_p^{\mathrm{T}} \mathbf{D}_p \boldsymbol{\varepsilon}_p + \delta\boldsymbol{\varepsilon}_s^{\mathrm{T}} \mathbf{D}_s \boldsymbol{\varepsilon}_s]\, \mathrm{d}\Omega = \int_\Omega [\delta\mathbf{u}]^{\mathrm{T}} \rho \ddot{\mathbf{u}}\, \mathrm{d}\Omega. \tag{21}$$

For a discretized FE domain, the displacement field can be expressed in terms of the nodal displacements $\mathbf{u}^a$ and the global shape functions $\hat{\mathbf{N}}_a$ [14] which are constructed from local shape functions $N_a$ and the accelerations can be also written in the same way:

$$\mathbf{u} = \sum_{a=1}^{np} \hat{\mathbf{N}}_a(\xi_1, \xi_2, \xi_3)\mathbf{u}^a, \qquad \ddot{\mathbf{u}} = \sum_{a=1}^{np} \hat{\mathbf{N}}_a(\xi_1, \xi_2, \xi_3)\ddot{\mathbf{u}}^a, \tag{22}$$

where $np$ is the total number of the node in the discretized domain and the virtual terms associated with the displacement and acceleration are

$$\delta\mathbf{u} = \sum_{a=1}^{np} \hat{\mathbf{N}}_a(\xi_1, \xi_2, \xi_3)\delta\mathbf{u}^a, \qquad \delta\ddot{\mathbf{u}} = \sum_{a=1}^{np} \hat{\mathbf{N}}_a(\xi_1, \xi_2, \xi_3)\delta\ddot{\mathbf{u}}^a, \tag{23}$$

The strain–displacement and virtual strain–displacement relationships can then be written as

$$\boldsymbol{\varepsilon} = \sum_{a=1}^{np} \hat{\mathbf{B}}^a \mathbf{u}^a, \qquad \delta\boldsymbol{\varepsilon} = \sum_{a=1}^{np} \hat{\mathbf{B}}^a \delta\mathbf{u}^a, \tag{24}$$

where $\hat{\mathbf{B}}^a$ is the global strain–displacement matrix which is constructed from local strain–displacement matrix $\mathbf{B}^a$.

Substituting equations (22)–(24) into equation (21) yields

$$\delta\mathbf{u}^{\mathrm{T}}[\mathbf{K}\mathbf{u} - \mathbf{M}\ddot{\mathbf{u}}] = \mathbf{0}. \tag{25}$$

Since the virtual displacement $\delta\mathbf{u}$ are arbitrary, the above equation may be written as

$$\mathbf{Ku} - \mathbf{M\ddot{u}} = 0. \tag{26}$$

A general solution to equation (26) may be written as

$$\mathbf{u} = \theta_k e^{i\omega_k t}. \tag{27}$$

Substituting equation (27) into equation (26) yields

$$[\mathbf{K} - \omega_k^2 \mathbf{M}]\phi_k = 0, \tag{28}$$

where $\phi_k$ is a set of displacement-type amplitude at the nodes otherwise known as the modal vector and $\omega_k$ is the *natural frequency* associated with the $k$th mode and $\mathbf{K} = \mathbf{A}_{e=1}^{nel}\,\mathbf{K}^{(e)}$ and $\mathbf{M} = \mathbf{A}_{e=1}^{nel}\,\mathbf{M}^{(e)}$ are global stiffness and mass matrices which contain contributions from the element stiffness and mass matrices formulated in the natural domain which, can be written as

$$\mathbf{K}^{ab(e)} = \int_{\tilde{\Omega}} [\tilde{\mathbf{B}}_p^{aT} \tilde{\mathbf{D}}_p^* \tilde{\mathbf{B}}_p^b + \tilde{\mathbf{B}}_s^{aT} \tilde{\mathbf{D}}_s^* \tilde{\mathbf{B}}_s^b]\, d\tilde{\Omega}, \qquad \mathbf{M}^{ab(e)} = \int_{\tilde{\Omega}} \tilde{\rho} \mathbf{N}_a^T \mathbf{N}_b\, d\Omega, \tag{29}$$

where the constitutive matrices $\tilde{\mathbf{D}}_p^*$ and $\tilde{\mathbf{D}}_s^*$ are given in equation (19). The matrices $\tilde{\mathbf{B}}_p^*$ and $\tilde{\mathbf{B}}_p^*$ are the in-plane and transverse shear strain–displacement matrices obtained from equation (12). Note that the explicit form of the mass matrix is dependent on the displacement field of the shell elements and the consistent mass matrix linking nodes $a$ and $b$ of an $n$-node shell element can be written as

$$\mathbf{M}^{ab(e)} = \int_{\tilde{\Omega}} \tilde{\rho} \begin{bmatrix} N_a N_b & 0 & 0 & 0 & 0 & 0 \\ 0 & N_a N_b & 0 & 0 & 0 & 0 \\ 0 & 0 & N_a N_b & 0 & 0 & 0 \\ 0 & 0 & 0 & \varrho_{23}^{ab} & \bar{\varrho}_{12}^{ab} & \bar{\varrho}_{13}^{ab} \\ 0 & 0 & 0 & \bar{\varrho}_{12}^{ab} & \varrho_{13}^{ab} & \bar{\varrho}_{23}^{ab} \\ 0 & 0 & 0 & \bar{\varrho}_{13}^{ab} & \bar{\varrho}_{23}^{ab} & \varrho_{12}^{ab} \end{bmatrix} d\tilde{\Omega}, \tag{30}$$

where $\tilde{\rho}$ is the density of the element material, $\varrho_{13}^{ab} = (\xi_3^2 h^a h^b)[\hat{d}_i^a \hat{d}_i^b + \hat{d}_j^a \hat{d}_j^b]/4$ and $\bar{\varrho}_{ij}^{ab} = -(\xi_3^2 h^a h^b \hat{d}_i^a \hat{d}_j^b)/4$ and $N_a$ is the shape function at node $a$.

It should be noted that the stiffness components associated with drilling degrees of freedom will be zero for the shell FEs having six degrees of freedom at each node if adjacent elements are coplanar or nearly coplanar. For this reason, the drilling degrees of freedom will be "linked" to the in-plane twisting mode of the mid-surface with a fictitious spring coefficient serving as a penalty parameter. From this concept, the torsional stiffness term was formed as described in reference [17] and added to the stiffness term in equation (29).

## 4. NUMERICAL EXAMPLES

Six numerical examples are considered in order to investigate the accuracy and reliability of the developed shell element based on the FE formulation described in the previous sections. For comparison purposes, an assumed natural nine-node plate element ANSP9 [20], a standard degenerated nine-node shell element LAG9 [17] and as assumed strain nine-node shell element ASL [19] are implemented and used to calculate new reference

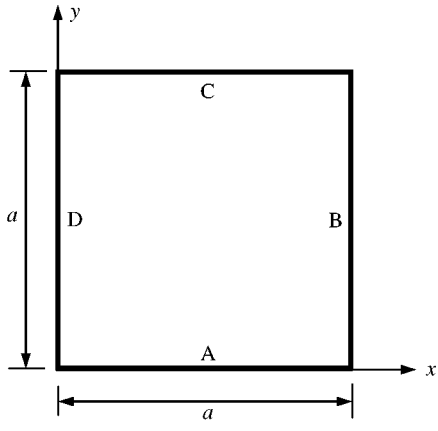


Figure 3. The geometry of square plate.

solutions for some examples. The numerical results are then compared with the exact solutions and the reference solutions which are available in the open literature. In this study, the plates are considered as zero-curvature shells.

### 4.1. SQUARE PLATE

A square plate is analyzed in order to examine the effect of using different boundary conditions on the free-vibration behaviour of the plate. For the purpose of concise identification, each set of the boundary conditions is denoted by four letters which stand for the four sides in the rectangular plate. The sequence begins with $x = 0$ and proceeds anti-clockwise around the plate such as A–B–C–D illustrated in Figure 3. The six boundary conditions used in this example are (a) S–S–S–S, (b) C–C–C–C, (c) C–C–C–F, (d) S–C–S–C, (e) S–C–S–S and (f) S–C–S–F where S, C and F stand for the simply supported, clamped and free boundary conditions respectively.

In addition to the six boundary conditions, two thickness-span ratios are used: $h/a = 0{\cdot}1$ and 0·01. In order to compare the present results with the existing reference solutions [21–26], several values of shear correction factors are employed according to the boundary conditions used: (a) S–S–S–S; $k_s = 0{\cdot}8330$, (b) C–C–C–C; $k_s = 0{\cdot}8330$, (c) C–C–C–F; $k_s = 0{\cdot}8220$, (d) S–C–S–C; $k_s = 0{\cdot}8601$, (e) S–C–S–S; $k_s = 0{\cdot}8601$ and (f) S–C–S–F; $k_s = 0{\cdot}8601$. The plates are discretized with a mesh of 100 nine-node elements. Note that an assumed natural nine-node plate element ANSP9 [20] and two shell elements LAG9 [17] and ASL9 [19] are used to produce new reference solutions.

In this example, the frequencies are presented in dimensionless form:

$$\Omega_n = \omega_n a(\rho/G)^{1/2},$$

where $\omega_n$ is the natural frequency of the plate, $a$ is the side length of the plate, $\rho$ is the mass density and the $G = E/2(1 + \nu)$ is the shear modulus in which $E$ is the elastic modulus and $\nu = 0{\cdot}3$ is the Poisson ratio.

(a) *S–S–S–S*: The simply supported plate has been frequently solved and several analytical solutions for this case are available: three-dimensional elasticity solution [21], RM thick plate theory and classical thin plate theory [24–28]. In this case, multiple frequencies are detected since the plate has a double symmetry. The natural frequencies are presented in Table 1.

TABLE 1

*The non-dimensionalized natural frequencies $\Omega_{mm}$ of a plate with the S/S/S/S boundary condition*

| $m$ | $n$ | ES | MC | TC | ANSP9 | ANSP9a | LAG9 | ASL9 | Present |
|---|---|---|---|---|---|---|---|---|---|
| *For the thickness* $h = 0{\cdot}1$ | | | | | | | | | |
| 1 | 1 | 0·932 | 0·9300 | 0·9632 | 0·9303 | 0·9303 | 0·9303 | 0·9303 | 0·9303 |
| 2 | 1 | 2·226 | 2·2190 | 2·4080 | 2·2198 | 2·2195 | 2·2194 | 2·2195 | 2·2195 |
| 2 | 2 | 3.421 | 3.4060 | 3.8530 | 3.4064 | 3.4054 | 3.4053 | 3.4054 | 3.4054 |
| 3 | 1 | 4·171 | 4·1490 | 4·8160 | 4·1542 | 4·1510 | 4·1509 | 4·1510 | 4·1510 |
| 3 | 2 | 5·239 | 5·2060 | 6·2610 | 5·2102 | 5·2053 | 5·2050 | 5·2054 | 5·2053 |
| 4 | 1 | — | 6·5200 | — | 6·5425 | 6·5270 | 6·5268 | 6·5270 | 6·5270 |
| 3 | 3 | 6·889 | 6·8340 | 8·6680 | 6·8414 | 6·8307 | 6·8295 | 6·8307 | 6·8307 |
| 4 | 2 | 7·511 | 7·4460 | 9·6320 | 7·4673 | 7·4484 | 7·4474 | 7·4484 | 7·4484 |
| 4 | 3 | — | 8·8960 | 22·0400 | 8·9178 | 8·8892 | 8·8861 | 8·8893 | 8·8892 |
| 5 | 1 | 9·268 | 9·1740 | 12·5210 | 9·2444 | 9·1928 | 9·1923 | 9·1928 | 9·1928 |
| 5 | 2 | — | 9·9840 | 13·9660 | 10·0510 | 9·9924 | 9·9900 | 9·9924 | 9·9924 |
| 4 | 4 | 10·890 | 10·7640 | 15·4110 | 10·7960 | 10·7430 | 10·7360 | 10·7430 | 10·7430 |
| *For the thickness* $h = 0{\cdot}01$ | | | | | | | | | |
| 1 | 1 | | 0·0963 | 0·0963 | 0·0963 | 0·0963 | 0·0963 | 0·0963 | 0·0963 |
| 2 | 1 | | 0·2406 | 0·2408 | 0·2406 | 0·2406 | 0·2406 | 0·2406 | 0·2406 |
| 2 | 2 | | 0·3848 | 0·3853 | 0·3848 | 0·3847 | 0·3846 | 0·3847 | 0·3847 |
| 3 | 1 | | 0·4809 | 0·4816 | 0·4814 | 0·4810 | 0·4808 | 0·4810 | 0·4811 |
| 3 | 2 | | 0·6249 | 0·6261 | 0·6253 | 0·6247 | 0·6243 | 0·6247 | 0·6247 |
| 4 | 1 | | 0·8167 | 0·8187 | 0·8198 | 0·8179 | 0·8167 | 0·8179 | 0·8179 |
| 3 | 3 | | 0·8647 | — | 0·8652 | 0·8639 | 0·8630 | 0·8639 | 0·8639 |
| 4 | 2 | | 0·9605 | — | 0·9633 | 0·9609 | 0·9593 | 0·9609 | 0·9609 |
| 4 | 3 | | 1·1997 | — | 1·2025 | 1·1988 | 1·1962 | 1·1989 | 1·1988 |

*Note*: ES: three-dimensional elasticity solutions [23]. MC: Reissner–Mindlin thick-plate theory solution [24, 25]. TC: thin-plate theory solution [24, 26]. ANSP9: assumed strain plate bending element solution using consistent mass [20]. ANSP9a: assumed strain plate bending element solution using lumped mass [20]. LAG9: nine-node shell element [17]. ASL9: assumed strain shell element [19].

(b) *C–C–C–C*: This is an inherently stiffer plate than the S–S–S–S plate. In this case, the multiple frequencies are also obtained because of its double symmetry. The natural frequencies are presented in Table 2.

(c) *C–C–C–F*: In this case, there is no double symmetry so multiple frequencies disappear. The mode shapes are particularly dominated by the free-boundary condition on one side of the plate. The natural frequencies are presented in Table 3.

(d) *S–C–S–C*: The overall mode shapes for this case are similar to those of the case S–S–S–S. However, the natural frequencies in this case are higher than those for case S–S–S–S. The natural frequencies are presented in Table 4.

(e) *S–C–S–S*: The overall mode shapes are similar to those of the cases S–S–S–S and S–C–S–C. The frequencies are a little higher than those of the case S–S–S–S but rather lower than those of the case S–C–S–C. The natural frequencies are presented in Table 5.

(f) *S–C–S–F*: This case has the lowest frequencies among the six cases. The overall mode shapes are similar to those of the case C–C–C–F but the frequencies in this case are lower than those of the case C–C–C–F. The natural frequencies are presented in Table 6.

From numerical results the natural strain shell elements shows a good performance and its results are in good agreement with the solutions obtained from the other shell elements. From the test, the plate with thickness $h = 0{\cdot}01$ has lower frequencies than the plate with thickness $h = 0{\cdot}1$.

TABLE 2

*The non-dimensionalized natural frequencies $\Omega_{mn}$ of a plate with the C/C/C/C boundary condition*

| $m$ | $n$ | MC | TC | ANSP9 | ANSP9a | LAG9 | ASL9 | Present |
|---|---|---|---|---|---|---|---|---|
| *For the thickness* $h = 0{\cdot}1$ | | | | | | | | |
| 1 | 1 | 1·594 | 1·756 | 1·5913 | 1·5912 | 1·5910 | 1·5912 | 1·5912 |
| 2 | 1 | 3·046 | 3·581 | 3·0406 | 3·0397 | 3·0393 | 3·0397 | 3·0397 |
| 2 | 2 | 4·285 | 5·280 | 4·2653 | 4·2631 | 4·2619 | 4·2631 | 4·2631 |
| 3 | 1 | 5·035 | 6·421 | 5·0341 | 5·0289 | 5·0282 | 5·0289 | 5·0289 |
| 1 | 3 | 5·078 | 6·451 | 5·0817 | 5·0763 | 5·0758 | 5·0763 | 5·0763 |
| 3 | 2 | | | 6·0891 | 6·0817 | 6·0797 | 6·0817 | 6·0817 |
| 4 | 1 | — | — | 7·4459 | 7·4258 | 7·4251 | 7·4258 | 7·4258 |
| 3 | 3 | — | — | 7·6934 | 7·6788 | 7·6750 | 7·6788 | 7·6788 |
| 4 | 2 | — | — | 8·2911 | 8·2675 | 8·1729 | 8·2675 | 8·2675 |
| 2 | 4 | — | — | 8·3669 | 8·3427 | 8·2645 | 8·3427 | 8·3427 |
| 4 | 3 | — | — | 9·7322 | 9·6978 | 9·6914 | 9·6978 | 9·6978 |
| *For the thickness* $h = 0{\cdot}01$ | | | | | | | | |
| 1 | 1 | 0·1754 | 0·1756 | 0·1754 | 0·1754 | 0·1754 | 1·7538 | 0·1754 |
| 2 | 1 | 0·3576 | 0·3581 | 0·3576 | 0·3575 | 0·3575 | 0·3575 | 0·3575 |
| 2 | 2 | 0·5274 | 0·5280 | 0·5268 | 0·5265 | 0·5264 | 0·5265 | 0·5265 |
| 3 | 1 | 0·6402 | 0·6421 | 0·6415 | 0·6407 | 0·6407 | 0·6407 | 0·6407 |
| 1 | 3 | 0·6432 | 0·6432 | 0·6446 | 0·6438 | 0·6438 | 0·6438 | 0·6438 |
| 3 | 2 | — | — | 0·8034 | 0·8021 | 0·8020 | 0·8021 | 0·8021 |
| 4 | 1 | — | — | 1·0296 | 1·0261 | 1·0261 | 1·0261 | 1·0261 |
| 3 | 3 | — | — | 1·0705 | 1·0679 | 1·0678 | 1·0679 | 1·0679 |
| 4 | 2 | — | — | 1·1818 | 1·1776 | 1·1775 | 1·1776 | 1·1776 |
| 2 | 4 | — | — | 1·1868 | 1·1825 | 1·1825 | 1·1826 | 1·1825 |
| 4 | 3 | — | — | 1·4436 | 1·4373 | 1·4371 | 1·4373 | 1·4373 |

*Note*: MC: Reissner–Mindlin thick-plate theory solution [24, 25]. TC: thin-plate theory solution [24, 26]. ANSP9: assumed strain plate bending element solution using consistent mass [20]. ANSP9a: assumed strain plate bending element solution using lumped mass [20]. LAG9: nine-node shell element [17]. ASL9: assumed strain shell element [19].

### 4.2. CIRCULAR PLATE

A circular plate with clamped boundaries is analyzed. Hinton *et al.* [29] analyzed this problem using three different types of boundary conditions: (a) symmetry conditions on both edges, (b) symmetry and antisymmetry conditions on each edge and (c) antisymmetry conditions on both edges. However, the entire plate is used to examine the free-vibration behaviour of the plate. The plate is discretized with a mesh of 108, nine-node elements. The resulting frequencies are presented in the dimensionless form

$$\Omega_n = \omega_n r^2 (\rho h/D)^{1/2},$$

where $\omega_n$ is the natural frequency of the plate, $r$ is the radius of the circular plate, $h$ the thickness of the plate, $\rho$ is the density of the material and the $D = Eh^3/12(1 - \nu^2)$ is the flexural rigidity of the plate in which $E$ is the elastic modulus and $\nu = 0{\cdot}3$ is the Poisson ratio. Two thickness-span ratios $h/2r = 0{\cdot}01$ and $0{\cdot}2$ are used in this study. Asymmetric and axisymmetric vibration modes are detected in this example and multiple frequencies are obtained from the axisymmetric modes. The result for the thickness–span ratio $h/2r = 0{\cdot}01$ is compared with the analytical solution [30]. It is shown that there are minor numerical

TABLE 3

*The non-dimensionalized natural frequencies $\Omega_n$ of a plate with the C/C/C/F boundary condition*

| $n$ | MC | TC | ANSP9 | ANSP9a | LAG9 | ASL9 | Present |
|---|---|---|---|---|---|---|---|
| *For the thickness* $h = 0{\cdot}1$ | | | | | | | |
| 1 | 1·089 | 1·171 | 1·0807 | 1·0807 | 1·0804 | 1·0807 | 1·0807 |
| 2 | 1·785 | 1·953 | 1·7440 | 1·7438 | 1·7429 | 1·7438 | 1·7438 |
| 3 | 2·673 | 3·094 | 2·6577 | 2·6569 | 2·6562 | 2·6569 | 2·6569 |
| 4 | 3·216 | 3·744 | 3·1979 | 3·1967 | 3·1955 | 3·1967 | 3·1967 |
| 5 | 3·318 | 3·938 | 3·2912 | 3·2902 | 3·2884 | 3·2902 | 3·2902 |
| 6 | 4·615 | 5·699 | 4·5605 | 4·5579 | 4·5548 | 4·5579 | 4·5579 |
| 7 | | | 4·7378 | 4·7328 | 4·7316 | 4·7328 | 4·7328 |
| 8 | — | — | 5·2521 | 5·2457 | 5·2444 | 5·2457 | 5·2457 |
| 9 | — | — | 5·3185 | 5·3129 | 5·3106 | 5·3129 | 5·3129 |
| 10 | — | — | 6·4016 | 6·3925 | 6·3385 | 6·3925 | 6·3925 |
| 11 | — | — | 6·4539 | 6·4456 | 6·4411 | 6·4456 | 6·4456 |
| 12 | — | — | 7·1630 | 7·1454 | 6·4802 | 7·1435 | 7·1454 |
| 13 | — | — | 7·6879 | 7·6669 | 7·6640 | 7·6669 | 7·6669 |
| 14 | — | — | 7·7092 | 7·6851 | 7·6837 | 7·6851 | 7·6851 |
| *For the thickness* $h = 0{\cdot}01$ | | | | | | | |
| 1 | 0·1171 | 0·1171 | 0·1166 | 0·1166 | 0·1166 | 0·1166 | 0·1166 |
| 2 | 0·1951 | 0·1953 | 0·1949 | 0·1949 | 0·1947 | 0·1949 | 0·1949 |
| 3 | 0·3093 | 0·3094 | 0·3082 | 0·3081 | 0·3079 | 0·3081 | 0·3081 |
| 4 | 0·3740 | 0·3744 | 0·3738 | 0·3736 | 0·3733 | 0·3736 | 0·3736 |
| 5 | 0·3931 | 0·3938 | 0·3924 | 0·3923 | 0·3920 | 0·3923 | 0·3923 |
| 6 | 0·5695 | 0·5699 | 0·5678 | 0·5674 | 0·5668 | 0·5674 | 0·5674 |
| 7 | — | — | 0·5963 | 0·5955 | 0·5953 | 0·5955 | 0·5955 |
| 8 | — | — | 0·6556 | 0·6547 | 0·6544 | 0·6547 | 0·6547 |
| 9 | — | — | 0·6835 | 0·6825 | 0·6822 | 0·6825 | 0·6825 |
| 10 | — | — | 0·8417 | 0·8402 | 0·8394 | 0·8402 | 0·8402 |
| 11 | — | — | 0·8605 | 0·8591 | 0·8583 | 0·8591 | 0·8591 |
| 12 | — | — | 0·9833 | 0·9800 | 0·9796 | 0·9800 | 0·9800 |
| 13 | — | — | 0·1040 | 1·0361 | 1·0357 | 1·0361 | 1·0361 |
| 14 | — | — | 0·1072 | 1·0684 | 1·0680 | 1·0684 | 1·0684 |

*Note*: MC: Reissner–Mindlin thick-plate theory solution [19, 20]. TC: thin-plate theory solution [19, 21]. ANSP9: assumed strain plate bending element solution using consistent mass [20]. ANSP9a: assumed strain plate bending element solution using lumped mass [20]. LAG9: nine-node shell element [17]. ASL9: assumed strain shell element [19].

discrepancies between the analytical solution and the present result. Some intermediate frequencies are calculated in the FE analysis. However, the frequencies obtained from the present shell elements show a very good agreement with the exact solutions in overall modes. The natural frequencies are presented in Table 7.

### 4.3. ELLIPTICAL PLATES

Liew [31] presented the vibration characteristics of elliptical plates with aspect ratios $a/b = 1$, 2, 3 and 4. The geometry of the plate is presented in Figure 4.

Since the results for the circular plate ($a/b = 1$) are already presented in Section 4.2, the results of three elliptical plates with aspect ratios $a/b = 2$, 3 and 4 are presented in this

TABLE 4

*The non-dimensionalized natural frequencies $\Omega_n$ of a plate with the S/C/S/C boundary condition*

| $n$ | MC | TC | FS | ANSP9 | ANSP9a | LAG9 | ASL9 | Present |
|---|---|---|---|---|---|---|---|---|
| *For the thickness* $h = 0{\cdot}1$ | | | | | | | | |
| 1 | 1·302 | 1·413 | 1·300 | 1·3002 | 1·3002 | 1·3001 | 1·3002 | 1·3002 |
| 2 | 2·398 | 2·671 | 2·394 | 2·3946 | 2·3941 | 2·3939 | 2·3941 | 2·3941 |
| 3 | 2·888 | 3·383 | 2·885 | 2·8861 | 2·8852 | 2·8850 | 2·8852 | 2·8852 |
| 4 | 3·852 | 4·615 | 3·839 | 3·8410 | 3·8394 | 3·8387 | 3·8394 | 3·8394 |
| 5 | 4·237 | 4·988 | 4·232 | 4·2362 | 4·2328 | 4·2324 | 4·2328 | 4·2328 |
| 6 | 4·939 | 6·299 | 4·936 | 4·9444 | 4·9394 | 4·9391 | 4·9394 | 4·9394 |
| 7 | — | — | — | 5·4626 | 5·4571 | 5·4559 | 5·4571 | 5·4571 |
| 8 | — | — | — | 5·7979 | 5·7913 | 5·7902 | 5·7913 | 5·7913 |
| 9 | — | — | — | 6·5768 | 6·5611 | 6·5605 | 6·5611 | 6·5611 |
| 10 | — | — | — | 7·2296 | 7·2173 | 7·2147 | 7·2173 | 7·2173 |
| 11 | — | — | — | 7·3315 | 7·3119 | 7·3115 | 7·3119 | 7·3119 |
| 12 | — | — | — | 7·6051 | 7·5854 | 7·5833 | 7·5854 | 7·5854 |
| 13 | — | — | — | 8·0972 | 8·0746 | 7·9898 | 8·0746 | 8·0746 |
| 14 | — | — | — | 9·1558 | 9·1256 | 9·1205 | 9·1256 | 9·1256 |
| *For the thickness* $h = 0{\cdot}01$ | | | | | | | | |
| 1 | 0·1411 | 0·1413 | 0·1411 | 0·1411 | 0·1411 | 0·1411 | 0·1411 | 0·1411 |
| 2 | 0·2668 | 0·2671 | 0·2668 | 0·2668 | 0·2668 | 0·2668 | 0·2668 | 0·2668 |
| 3 | 0·3377 | 0·3383 | 0·3376 | 0·3378 | 0·3377 | 0·3377 | 0·3377 | 0·3377 |
| 4 | 0·4608 | 0·4615 | 0·4604 | 0·4607 | 0·4604 | 0·4604 | 0·4604 | 0·4604 |
| 5 | 0·4979 | 0·4988 | 0·4977 | 0·4984 | 0·4980 | 0·4980 | 0·4980 | 0·4980 |
| 6 | 0·6279 | 0·6299 | 0·6279 | 0·6295 | 0·6287 | 0·6287 | 0·6287 | 0·6287 |
| 7 | — | — | — | 0·6827 | 0·6820 | 0·6820 | 0·6820 | 0·6820 |
| 8 | — | — | — | 0·7539 | 0·7529 | 0·7528 | 0·7529 | 0·7529 |
| 9 | — | — | — | 0·8321 | 0·8301 | 0·8301 | 0·8301 | 0·8301 |
| 10 | — | — | — | 0·9725 | 0·9705 | 0·9705 | 0·9705 | 0·9705 |
| 11 | — | — | — | 0·1008 | 1·0052 | 1·0052 | 1·0052 | 1·0052 |
| 12 | — | — | — | 0·1019 | 1·0158 | 1·0158 | 1·0158 | 1·0158 |
| 13 | — | — | — | 0·1146 | 1·1416 | 1·1415 | 1·1416 | 1·1416 |
| 14 | — | — | — | 0·1269 | 1·2623 | 1·2623 | 1·2623 | 1·2623 |

*Note*: MC: Reissner–Mindlin thick-plate theory solution [24, 25]. TC: thin-plate theory solution [24, 26]. FS: finite strip solution [25]. ANSP9: assumed strain plate bending element solution using consistent mass [20]. ANSP9a: assumed strain plate bending element solution using lumped mass [20]. LAG9: nine-node shell element [17]. ASL9: assumed strain shell element [19].

section. The resulting frequencies are presented in the dimensionless form.

$$\Omega_n = \omega_n a^2 (\rho h/D)^{1/2},$$

where $\omega_n$ is the natural frequency of the plate, $a$ is the radius of the elliptical plates in the $x$ direction, $\rho$ is the density of the material, $h$ is the thickness of the plate, and the $D = Eh^3/12(1 - v^2)$ is the flexural rigidity of the plate in which $E$ is the elastic modulus and $v = 0{\cdot}3$ is the Poisson ratio. The thickness–span ratio is assumed as $h/2b = 0{\cdot}01$ since there is no information of aspect ratio presented in reference [31] and the plate is discretized with a mesh of 400 FEs for analysis. All units are assumed to be consistent. The frequencies calculated by using the present shell elements with the aspect ratio show good agreement with Liew's results although there are some discrepancies in the higher mode. As a reference solution, the FE solution obtained by using the shell element S9R5 of the ABAQUS [32] is

TABLE 5

*The non-dimensionalized natural frequencies $\Omega_n$ of a plate with the S/C/S/S boundary condition*

| $n$ | MC | TC | FS | ANSP9 | ANSP9a | LAG9 | ASL9 | Present |
|---|---|---|---|---|---|---|---|---|
| *For the thickness* $h = 0{\cdot}1$ | | | | | | | | |
| 1 | 1·092 | 1·154 | 1·092 | 1·0919 | 1·0918 | 1·0918 | 1·0918 | 1·0918 |
| 2 | 2·298 | 2·521 | 2·296 | 2·2969 | 2·2965 | 2·2964 | 2·2965 | 2·2965 |
| 3 | 2·543 | 2·862 | 2·542 | 2·5425 | 2·5420 | 2·5419 | 2·5420 | 2·5420 |
| 4 | 3·616 | 4·203 | 3·611 | 3·6121 | 3·6108 | 3·6105 | 3·6108 | 3·6108 |
| 5 | 4·187 | 4·893 | 4·184 | 4·1892 | 4·1859 | 4·1857 | 4·1859 | 4·1859 |
| 6 | 4·543 | 5·525 | 4·541 | 4·5475 | 4·5434 | 4·5432 | 4·5434 | 4·5434 |
| 7 | — | — | — | 5·3267 | 5·3216 | 5·3208 | 5·3216 | 5·3216 |
| 8 | — | — | — | 5·4967 | 5·4910 | 5·4903 | 5·4910 | 5·4910 |
| 9 | — | — | — | 6·5521 | 6·5365 | 6·5361 | 6·5365 | 6·5365 |
| 10 | — | — | — | 6·9368 | 6·9192 | 6·9189 | 6·9192 | 6·9192 |
| 11 | — | — | — | 7·0252 | 7·0137 | 7·0118 | 7·0137 | 7·0137 |
| 12 | — | — | — | 7·5256 | 7·5063 | 7·5048 | 7·5854 | 7·5063 |
| 13 | — | — | — | 7·7762 | 7·7554 | 7·7540 | 7·7554 | 7·7554 |
| 14 | — | — | — | 9·0236 | 8·9942 | 8·9902 | 8·9942 | 8·9942 |
| *For the thickness* $h = 0{\cdot}01$ | | | | | | | | |
| 1 | 0·1153 | 0·1154 | 0·1153 | 0·1153 | 0·1153 | 0·1153 | 0·1153 | 0·1153 |
| 2 | 0·2521 | 0·2521 | 0·2519 | 0·2519 | 0·2519 | 0·2519 | 0·2519 | 0·2519 |
| 3 | 0·2858 | 0·2862 | 0·2858 | 0·2859 | 0·2858 | 0·2858 | 0·2858 | 0·2858 |
| 4 | 0·4190 | 0·4203 | 0·4195 | 0·4197 | 0·4195 | 0·4195 | 0·4195 | 0·4195 |
| 5 | 0·4889 | 0·4893 | 0·4883 | 0·4890 | 0·4886 | 0·4886 | 0·4886 | 0·4886 |
| 6 | 0·5533 | 0·5525 | 0·5513 | 0·5522 | 0·5516 | 0·5516 | 0·5516 | 0·5516 |
| 7 | — | — | — | 0·6518 | 0·6511 | 0·6511 | 0·6511 | 0·6511 |
| 8 | — | — | — | 0·6862 | 0·6854 | 0·6854 | 0·6854 | 0·6854 |
| 9 | — | — | — | 0·8255 | 0·8235 | 0·8235 | 0·8235 | 0·8235 |
| 10 | — | — | — | 0·9159 | 0·9136 | 0·9136 | 0·9136 | 0·9136 |
| 11 | — | — | — | 0·9162 | 0·9142 | 0·9142 | 0·9142 | 0·9142 |
| 12 | — | — | — | 0·9840 | 0·9815 | 0·9815 | 0·9815 | 0·9815 |
| 13 | — | — | — | 0·1051 | 1·0478 | 1·0478 | 1·0478 | 1·0478 |
| 14 | — | — | — | 0·1245 | 1·2404 | 1·2623 | 1·2623 | 1·2404 |

*Note*: MC: Reissner–Mindlin thick-plate theory solution [24, 25]. TC: thin-plate theory solution [24, 26]. FS: finite strip solution [25]. ANSP9: assumed strain plate bending element solution using consistent mass [20]. ANSP9a: assumed strain plate bending element solution using lumped mass [20]. LAG9: nine-node shell element [17]. ASL9: assumed strain shell element [19].

also provided. The natural frequencies and mode shapes of the elliptical plates are presented in Figures 5, 6 and 7 and Table 8 respectively.

### 4.4. DOUBLY CURVED SHELL

In this example, the effect of double curvature on the natural frequencies is investigated. The mid-surface of the shell is defined in the following equation:

$$x = -\frac{1}{2}\left(\frac{x^2}{R_x} + \frac{y^2}{R_y}\right)$$

TABLE 6

*The non-dimensionalized natural frequencies $\Omega_n$ of a plate with the S/C/S/F boundary condition*

| $n$ | MC | TC | FS | ANSP9 | ANSP9a | LAG9 | ASL9 | Present |
|---|---|---|---|---|---|---|---|---|
| *For the thickness* $h = 0{\cdot}1$ | | | | | | | | |
| 1 | 0·603 | 0·619 | 0·598 | 0·5977 | 0·5977 | 0·5975 | 0·5977 | 0·5977 |
| 2 | 1·495 | 1·613 | 1·483 | 1·4836 | 1·4835 | 1·4827 | 1·4835 | 1·4835 |
| 3 | 1·900 | 2·035 | 1·884 | 1·8848 | 1·8845 | 1·8840 | 1·8845 | 1·8845 |
| 4 | 2·744 | 3·075 | 2·720 | 2·7220 | 2·7214 | 2·7200 | 2·7214 | 2·7214 |
| 5 | 3·073 | 3·533 | 3·057 | 3·0595 | 3·0584 | 3·0574 | 3·0584 | 3·0584 |
| 6 | 3·855 | 4·421 | 3·827 | 3·8329 | 3·8299 | 3·8288 | 3·8299 | 3·8299 |
| 7 | — | — | — | 4·1892 | 4·1872 | 4·1846 | 4·1872 | 4·1872 |
| 8 | — | — | — | 4·5709 | 4·5671 | 4·5652 | 4·5671 | 4·5671 |
| 9 | — | — | — | 5·1551 | 5·1489 | 5·1479 | 5·1489 | 5·1489 |
| 10 | — | — | — | 5·9013 | 5·8948 | 5·8911 | 5·8948 | 5·8948 |
| 11 | — | — | — | 6·1497 | 6·1415 | 6·1381 | 6·1415 | 6·1415 |
| 12 | — | — | — | 6·2367 | 6·2218 | 6·2200 | 6·2218 | 6·2218 |
| 13 | — | — | — | 6·8765 | 6·8598 | 6·8573 | 6·8598 | 6·8598 |
| 14 | — | — | — | 7·6122 | 7·5885 | 7·5874 | 7·5885 | 7·5885 |
| *For the thickness* $h = 0{\cdot}01$ | | | | | | | | |
| 1 | 0·0622 | 0·0619 | 0·0619 | 0·0619 | 0·0619 | 0·0618 | 0·0619 | 0·0619 |
| 2 | 0·1612 | 0·1613 | 0·1611 | 0·1612 | 0·1612 | 0·1610 | 0·1612 | 0·1612 |
| 3 | 0·2045 | 0·2035 | 0·2033 | 0·2034 | 0·2033 | 0·2032 | 0·2033 | 0·2033 |
| 4 | 0·3075 | 0·3075 | 0·3070 | 0·3071 | 0·3070 | 0·3067 | 0·3070 | 0·3070 |
| 5 | 0·3528 | 0·3533 | 0·3526 | 0·3528 | 0·3527 | 0·3525 | 0·3527 | 0·3527 |
| 6 | 0·4438 | 0·4421 | 0·4413 | 0·4420 | 0·4417 | 0·4415 | 0·4417 | 0·4417 |
| 7 | — | — | — | 0·5024 | 0·5021 | 0·5015 | 0·5021 | 0·5021 |
| 8 | — | — | — | 0·5454 | 0·5459 | 0·5446 | 0·5449 | 0·5449 |
| 9 | — | — | — | 0·6411 | 0·6402 | 0·6399 | 0·6402 | 0·6402 |
| 10 | — | — | — | 0·7438 | 0·7430 | 0·7422 | 0·7430 | 0·7430 |
| 11 | — | — | — | 0·7786 | 0·7768 | 0·7765 | 0·7768 | 0·7768 |
| 12 | — | — | — | 0·7911 | 0·7899 | 0·7891 | 0·7899 | 0·7899 |
| 13 | — | — | — | 0·8809 | 0·8788 | 0·8783 | 0·8788 | 0·8788 |
| 14 | — | — | — | 1·0288 | 1·0252 | 1·0248 | 1·0252 | 1·0252 |

*Note*: MC: Reissner–Mindlin thick-plate theory solution [24, 25]. TC: thin-plate theory solution [24, 26]. FS: finite strip solution [25]. ANSP9: assumed strain plate bending element solution using consistent mass [20]. ANSP9a: assumed strain plate bending element solution using lumped mass [20]. LAG9: nine-node shell element [17]. ASL9: assumed strain shell element [19].

in which $R_x$ and $R_y$ are the radii of curvature in the $x$ and $y$ directions respectively. The shell has curvilinear planform. Two kinds of curvilinear planforms are considered, namely, the circular ($a/b = 1$) and elliptical ($a/b = 2$) planforms. The geometry of the shell is presented in Figure 8. The shell is assumed to be clamped on its circular or elliptical circumference. The effect of Gaussian curvature ($1/R_xR_y$) is investigated by varying the curvature ratio ($R_y/R_x$) with combination of the wide ranges of shallowness ratio ($2b/R_y$). The Poisson ratio of shells is $v = 0{\cdot}3$ and its thickness ratio is taken as $2a/h = 100{\cdot}0$. The resulting frequencies are presented in the dimensionless form

$$\Omega_n = 4\omega_n ab(\rho h/D)^{1/2},$$

TABLE 7

*The non-dimensionalized natural frequencies $\Omega_n$ of a clamped circular plate*

| Mode | Aspect ratio $h/a = 0{\cdot}01$ | | | | Aspect ratio $h/a = 0{\cdot}2$ | | |
|---|---|---|---|---|---|---|---|
| $n$ | AS | LAG9 | ASL9 | Present | LAG9 | ASL | Present |
| 1 | 10·2158 | 10·2135 | 10·2129 | 10·2129 | 7·49398 | 7·49388 | 7·49382 |
| 2 | 21·2600 | 21·2341 | 21·2311 | 21·3110 | 13·04010 | 13·04010 | 13·04000 |
| — | — | — | — | — | — | — | — |
| 3 | 34·8800 | 34·7925 | 34·7816 | 34·7816 | 18·62370 | 18·62300 | 18·62270 |
| — | — | 34·8027 | 34·7915 | 34·7915 | 18·62590 | 18·62520 | 18·62500 |
| 4 | 39·7710 | 39·6796 | 39·6766 | 39·6766 | 20·52050 | 20·52130 | 20·52100 |
| 5 | 51·0400 | 50·8591 | 50·8348 | 50·8348 | 24·29180 | 24·29140 | 24·29100 |
| — | — | — | — | — | — | — | — |
| 6 | 60·8200 | 60·6797 | 60·6761 | 60·6761 | 27·34810 | 27·35060 | 27·35030 |
| — | — | — | — | — | — | — | — |
| 7 | 69·6659 | 69·3585 | 69·3028 | 69·3027 | 29·98000 | 29·98520 | 29·98480 |
| — | — | 69·3637 | 69·3379 | 69·3379 | 29·98340 | 29·98690 | 29·98650 |
| 8 | 84·5800 | 84·3196 | 84·2999 | 84·2999 | 30·45530 | 33·92340 | 33·92290 |
| — | — | 84·3800 | 84·3835 | 84·3853 | — | 33·92610 | 33·92560 |
| 9 | 111·0100 | 88·9752 | 88·9848 | 88·9848 | 33·91490 | 35·12680 | 35·12630 |
| 10 | 140·1080 | 90·2597 | 90·2078 | 90·2078 | 35·63310 | 35·65090 | 35·65040 |
| — | | — | — | — | — | — | — |
| 11 | | 110·5830 | 110·5630 | 110·5630 | 40·29730 | 40·31720 | 40·31660 |
| — | | — | — | — | — | — | — |
| 12 | | 113·5440 | 113·4890 | 113·4890 | 41·19330 | 41·23920 | 41·23850 |
| — | | 113·5570 | 113·5020 | 113·5020 | 41·19470 | 41·24180 | 41·24120 |
| 13 | | 119·8420 | 119·8480 | 119·8480 | 42·00430 | 42·01420 | 42·01360 |
| — | | — | — | — | — | — | — |
| 14 | | 139·2750 | 139·2220 | 139·2220 | 44·78240 | 44·78420 | 44·78340 |
| — | | — | — | — | — | — | — |
| 15 | | 139·3700 | 139·2280 | 139·2280 | 45·12300 | 45·01030 | 45·00960 |
| — | | 139·3920 | 139·3760 | 139·3760 | | | |

*Note.* AS: analytical solutions [30]. LAG9: nine-node shell element [17]. ASL9: assumed strain shell element [19]. — multiple frequencies associated with axisymmetric modes.

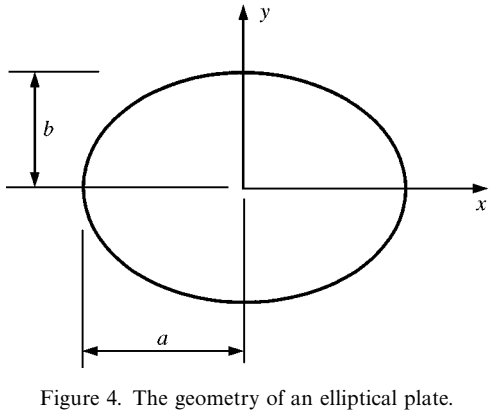


Figure 4. The geometry of an elliptical plate.

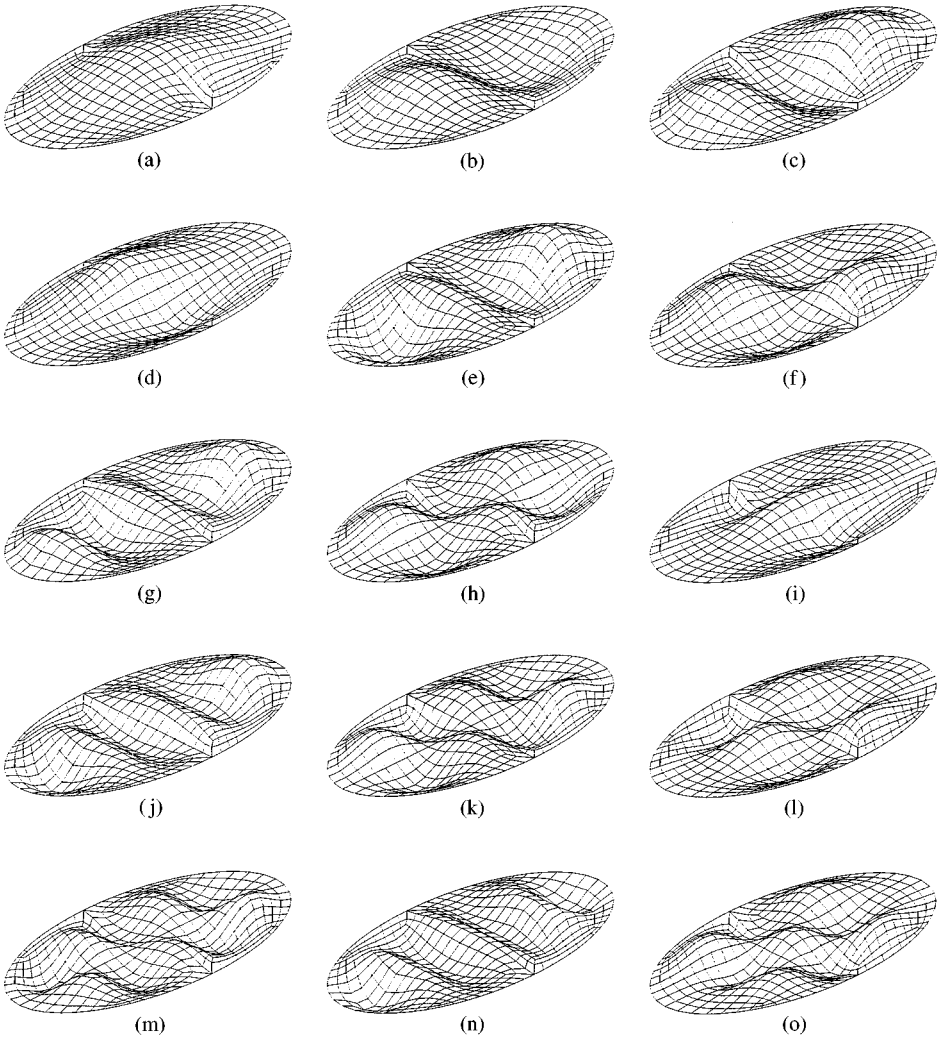


Figure 5. A clamped elliptical plate with aspect ratio $a/b = 2$: (a) mode 1–(o) mode 15.

where $\omega_n$ is the natural frequency of the plate, $a$ is the radius of the elliptical plates in the $x$ direction, $b$ is the radius of the elliptical plates in the $y$ direction, $\rho$ is the density of the material, $h$ is the thickness of the shell and the $D = Eh^3/12(1 - v^2)$ is the flexural rigidity of the plate in which $E$ is the elastic modulus and $v = 0{\cdot}3$ is the Poisson ratio. The thickness–span ratio is taken as $h/2a = 0{\cdot}01$ and the plate is discretized with a mesh of 400 FEs for analysis. All units are assumed to be consistent. The present result is in good agreement with a reference solution [33] with lower curvature ($2b/R_y$) but there are some discrepancies in case of shells with higher curvature. To clarify this discrepancies between the present element and the reference solution [33], the shell element S9R5 of the ABAQUS [32] is used to produce new FE reference solution. The present results are in good agreement with the FE solutions obtained with the ABAQUS. From this study, it was found that the curvature of the shell greatly affects the free-vibration behaviour. The fundamental frequencies of the shell are presented in Tables 9 and 10.

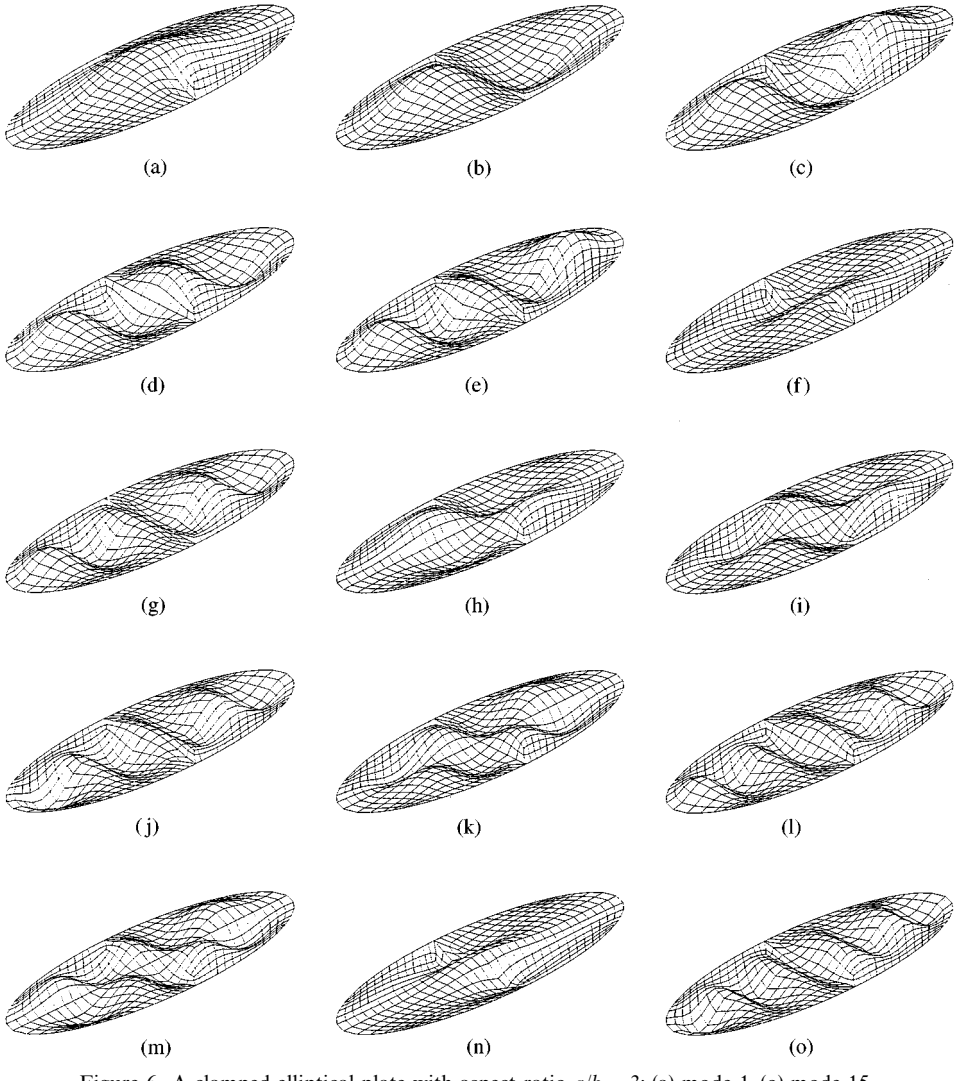


Figure 6. A clamped elliptical plate with aspect ratio $a/b = 3$: (a) mode 1–(o) mode 15.

### 4.5. CLAMPED CYLINDRICAL SHELL PANEL

A clamped cylindrical shell is analyzed. It was tested experimentally by Nath [34] and was also solved numerically by various methods [35–37]. The following material properties are used: elastic modulus $E = 10^7$, the Poisson ratio $v = 0{\cdot}33$ and the mass density of $\rho = 0{\cdot}096$. The thickness of the shell is taken as $h = 0{\cdot}013$ and a $10 \times 10$ FE mesh is used for analysis. All units are assumed to be consistent. The geometry of the shell is illustrated in Figure 9.

The two shell elements LAG9 [17], ASL9 [19] are used to produce a reference solutions and the results are presented in Figures 10 and 11 and Table 11. The frequencies obtained using the element LAG9 are higher than those obtained using the elements ASL9 and the present element. The present element produces the best agreement with the solution which is based on the higher order theory [36].

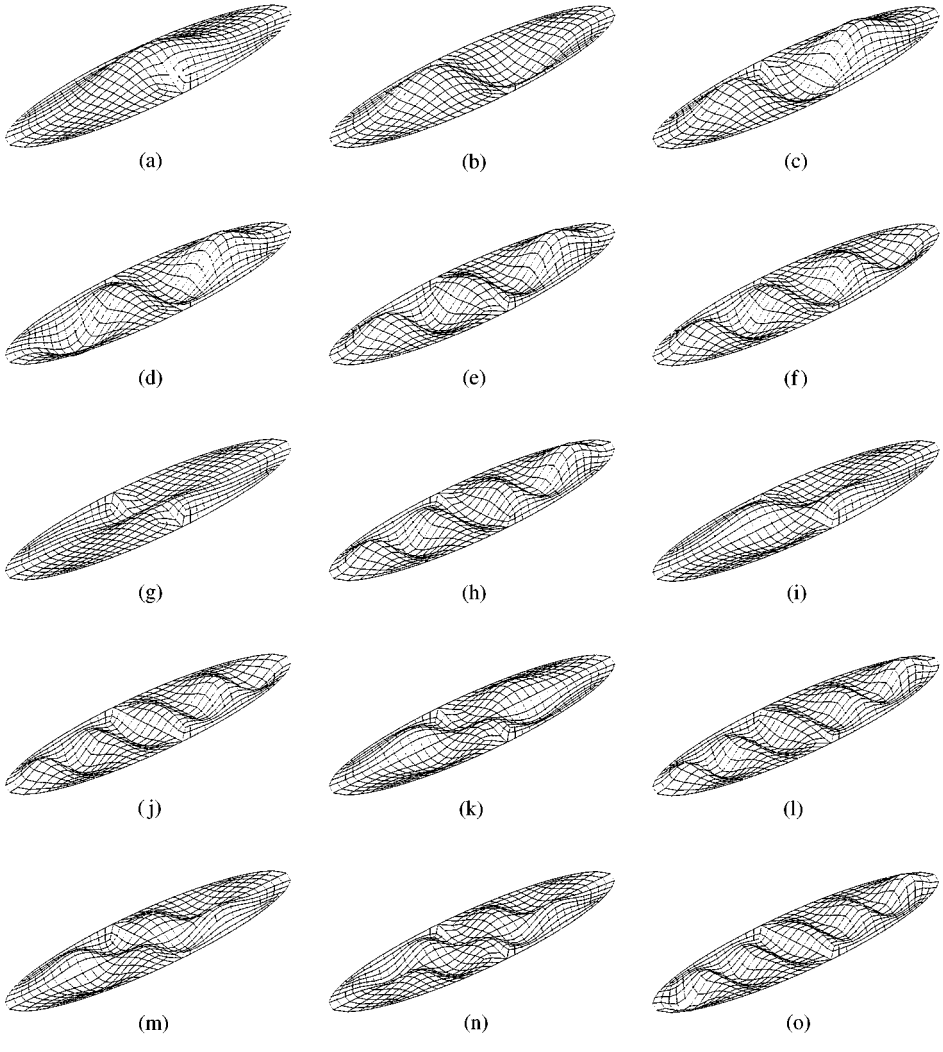


Figure 7. A clamped elliptical plate with aspect ratio $a/b = 4$: (a) mode 1–(o) mode 15.

### 4.6. CYLINDRICAL SHELL: CURVED FAN BLADE

The vibrations of cylindrical shells have been frequently studied because of the relationship to practical vibration problems such as turbine engine blade. Lee *et al.* [38] investigated the behaviour of this structure using the Ritz method based on classical thin-shallow-shell theory in which the different polynomial terms are used. In addition, the effects of the aspect ratio ($a/b$), shallowness ratio ($b/R$) and width–thickness ratio ($b/h$) on the frequencies were also investigated by them. In order to investigate the effect of span–thickness ratio on the natural frequencies and mode shapes, a moderately thin ($b/h = 100$) and shallow shell ($b/R = 0{\cdot}5$) is used. First, the effect of aspect ratio ($a/b$) on the frequency is investigated with two aspect ratios: ($a/b$) = 1 and 5. Note that Lim and Liew [39] also investigated the same problem and it is used here as reference solution in this

TABLE 8

*The non-dimensionalized natural frequencies $\Omega_n$ of a clamped eliptical plates*

| Mode | $a/b = 2$ | | | $a/b = 3$ | | | $a/b = 4$ | | |
|---|---|---|---|---|---|---|---|---|---|
| $n$ | Ref | Abaqus | Present | Ref | Abaqus | Present | Ref | Abaqus | Present |
| 1 | 27·4773 | 27·2460 | 27·2841 | 56·8995 | 56·1096 | 56·3842 | 97·5984 | 95·7492 | 96·3561 |
| 2 | 39·4976 | 39·2112 | 39·3187 | 71·5902 | 70·1736 | 70·9595 | 115·6080 | 112·7570 | 113·8980 |
| 3 | 55·9773 | 55·5036 | 55·6492 | 90·2380 | 88·0596 | 89·2972 | 137·2690 | 133·5000 | 134·9390 |
| 4 | 69·8557 | 69·1572 | 69·3343 | 113·2660 | 109·6860 | 111·5840 | 164·3250 | 157·2960 | 159·5900 |
| 5 | 77·0443 | 76·2480 | 76·4236 | 140·7460 | 135·5400 | 137·9990 | 195·3400 | 184·7760 | 187·9870 |
| 6 | 88·0472 | 86·8140 | 87·2420 | 150·0890 | 146·4360 | 147·6710 | 255·0950 | 215·7240 | 220·2470 |
| 7 | — | 101·5360 | 101·6943 | — | 165·8040 | 168·6610 | — | 250·6680 | 254·0450 |
| 8 | — | 108·1620 | 108·7374 | — | 168·1440 | 171·2220 | — | 250·6680 | 256·4610 |
| 9 | — | 130·2000 | 130·6763 | — | 193·7880 | 198·0190 | — | 278·1120 | 283·2320 |
| 10 | — | 131·3400 | 131·4431 | — | 200·5920 | 203·6420 | — | 289·6200 | 296·6990 |
| 11 | — | 133·1640 | 133·9560 | — | 221·9760 | 228·1300 | — | 310·3320 | 315·4470 |
| 12 | — | 153·6360 | 154·6886 | — | 239·8440 | 242·9620 | — | 333·0600 | 340·9870 |
| 13 | — | 162·0600 | 162·9953 | — | 253·4160 | 261·6840 | — | 343·8240 | 354·7230 |
| 14 | — | 165·5760 | 165·6098 | — | 277·2000 | 280·4390 | — | 380·7600 | 389·1430 |
| 15 | — | 180·7920 | 182·0875 | — | 283·3200 | 286·6140 | — | 381·0840 | 389·3490 |

*Note.* Ref: analytical solution [31]. Abaqus: FE solution using Abaqus [32].

example. A $10 \times 10$ FE mesh is used to model the entire shell. The shell geometry is presented in Figure 12. The result is expressed in non-dimensional form as

$$\Omega = \omega_n a^2 \sqrt{\frac{\rho h}{D}},$$

where $\omega_n$ is the natural frequency of the shell, $a$ is the width of the shell, $\rho$ is the density of the material, $h$ is the thickness of the shell and the flexural rigidity is $D = Eh^3/12(1 - v^2)$ in which $E$ is the elastic modulus and $v = 0{\cdot}3$ is the Poisson ratio. The results are compared with the solution obtained by the Ritz method where six and five polynomial terms are used in the $x$ and $y$ directions respectively. From the test, the larger aspect ratio produces the lower frequency and quite different mode shapes are observed. The natural frequencies and the mode shapes are presented in Table 12 and Figures 13 and 14.

## 5. CONCLUSIONS

The assumed natural strain nine-node Lagrangian shell element is developed and used to assess the vibration behaviour of shell structures. The accuracy and efficiency of the proposed shell FE formulation are tested by six numerical examples. From the numerical results, the shell element based on the proposed formulation has performed well in most situations and the results are very close to the theoretical solutions and have a good agreement with the other reference solutions. It is shown that the present shell element is applicable to most shell structures which are either the thick or thin case.

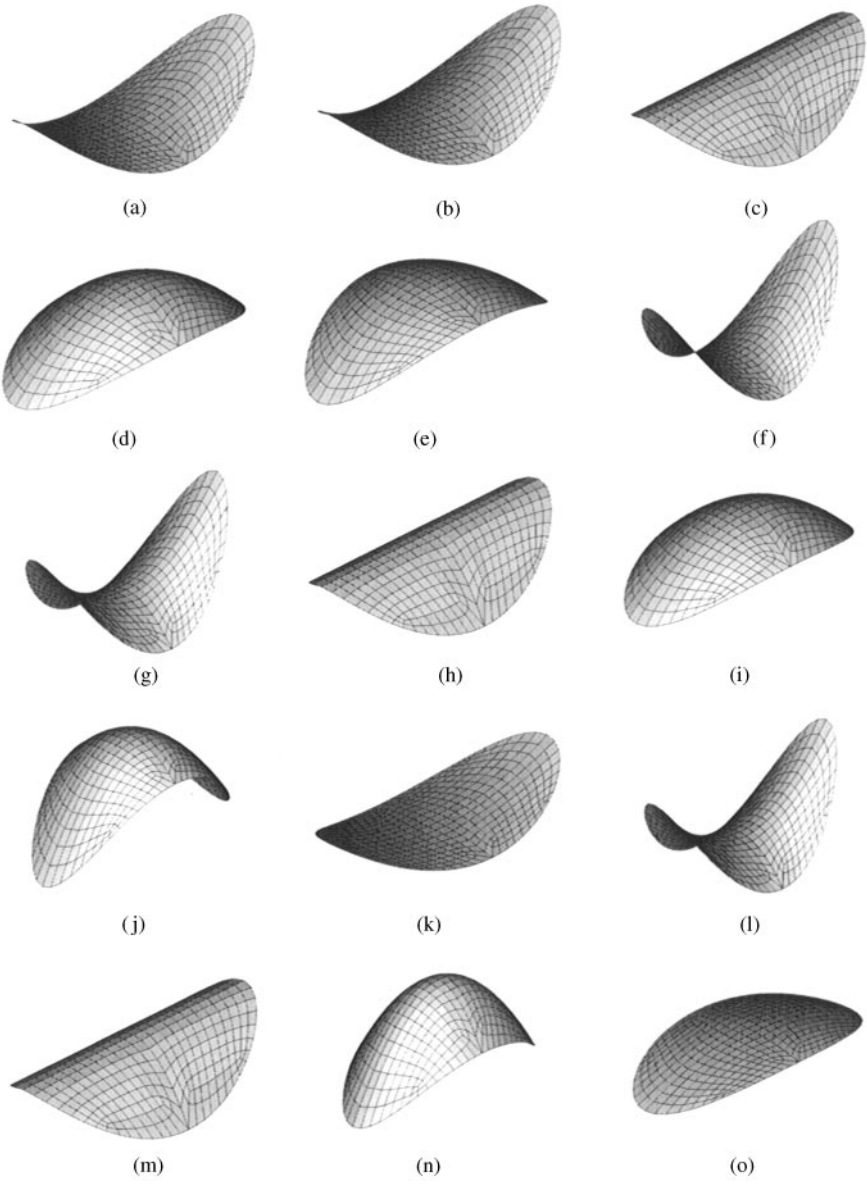


Figure 8. The shell geometries with respect to the parameters $(2b/R_y, R_y/R_x)$: (a) (0·1, −1·0), (b) (0·1, −1·5), (c) (0·1, 0·0), (d) (0·1, 0·5), (e) (0·1, 1·0), (f) (0·3, −1·0), (g) (0·3, −0·5), (h) (0·3, 0·0), (i) (0·3, 0·5), (j) (0·3, 1·0), (k) (0·5, −1·0), (l) (0·5, −0·5), (m) (0·5, 0·0), (n) (0·5, 0·5) and (o) (0·5, 1·0).

TABLE 9

*Natural frequencies $\omega_n$ of fully clamped doubly curved shallow shell with circular platform*

| | | | Mode | | | | | | | |
|---|---|---|---|---|---|---|---|---|---|---|
| $2b/R_y$ | $R_y/R_z$ | | 1 | 2 | 3 | 4 | 5 | 6 | 7 | 8 |
| 0·1 | − 1·0 | Pre | 54·039 | 89·795 | 89·795 | 140·78 | 142·68 | 160·77 | 204·86 | 204·86 |
| | | Refa | 54·038 | 89·803 | 89·803 | 140·77 | 142·75 | 160·81 | 204·94 | 204·94 |
| | | Refb | 54·100 | 90·016 | 90·025 | 141·30 | 143·25 | 161·43 | 205·94 | 205·97 |
| | − 0·5 | Pre | 50·055 | 86·729 | 89·487 | 140·28 | 141·33 | 160·09 | 204·28 | 204·29 |
| | | Refa | 50·054 | 86·736 | 89·496 | 140·27 | 141·40 | 160·13 | 204·36 | 204·37 |
| | | Refb | 50·111 | 86·954 | 89·689 | 140·79 | 141·87 | 160·73 | 205·33 | 205·35 |
| | 0·0 | Pre | 50·158 | 86·066 | 89·760 | 140·54 | 140·96 | 160·23 | 204·26 | 204·27 |
| | | Refa | 50·160 | 86·074 | 89·770 | 140·53 | 141·03 | 160·27 | 204·34 | 204·36 |
| | | Refb | 50·268 | 86·300 | 89·958 | 141·06 | 141·50 | 160·87 | 205·31 | 205·33 |
| | 0·5 | Pre | 54·345 | 87·875 | 90·607 | 141·54 | 141·64 | 161·13 | 204·82 | 204·82 |
| | | Refa | 54·350 | 87·883 | 90·619 | 141·54 | 141·71 | 161·17 | 204·90 | 204·91 |
| | | Refb | 54·411 | 88·120 | 90·827 | 142·09 | 142·19 | 161·80 | 205·89 | 205·91 |
| | 1·0 | Pre | 61·729 | 92·005 | 92·005 | 143·28 | 143·29 | 162·85 | 205·93 | 205·93 |
| | | Refa | 61·733 | 92·016 | 92·016 | 143·27 | 143·36 | 162·89 | 206·01 | 206·02 |
| | | Refb | 61·811 | 92·263 | 92·278 | 143·87 | 143·89 | 163·58 | 207·06 | 207·08 |
| 0·3 | − 1·0 | Pre | 111·790 | 121·460 | 121·460 | 153·72 | 168·59 | 178·16 | 217·57 | 217·57 |
| | | Refa | 111·790 | 121·460 | 121·460 | 153·71 | 168·64 | 178·20 | 217·61 | 217·61 |
| | | Refb | 54·100 | 90·016 | 90·025 | 141·30 | 143·25 | 161·43 | 205·94 | 205·97 |
| | − 0·5 | Pre | 94·021 | 100·220 | 119·390 | 149·67 | 155·99 | 174·85 | 212·53 | 212·98 |
| | | Refa | 94·022 | 100·220 | 119·400 | 149·66 | 156·04 | 174·90 | 212·58 | 213·07 |
| | | Refb | 94·336 | 100·850 | 119·830 | 150·56 | 157·37 | 175·74 | 214·31 | 214·73 |
| | 0·0 | Pre | 93·484 | 94·807 | 121·300 | 151·75 | 152·48 | 176·97 | 212·40 | 212·50 |
| | | Refa | 93·490 | 94·814 | 121·310 | 151·75 | 152·54 | 177·02 | 212·46 | 212·61 |
| | | Refb | 93·823 | 95·505 | 121·680 | 152·69 | 153·92 | 177·77 | 214·19 | 214·30 |
| | 0·5 | Pre | 108·600 | 111·460 | 127·010 | 159·70 | 159·90 | 183·22 | 217·27 | 217·31 |
| | | Refa | 108·610 | 111·470 | 127·030 | 159·77 | 159·91 | 183·28 | 217·38 | 217·38 |
| | | Refb | 109·420 | 111·880 | 127·620 | 161·12 | 161·17 | 184·46 | 219·29 | 219·34 |
| | 1·0 | Pre | 135·540 | 135·540 | 138·790 | 172·98 | 172·99 | 197·15 | 226·50 | 226·50 |
| | | Refa | 135·560 | 135·560 | 138·810 | 173·00 | 173·06 | 197·20 | 226·60 | 226·60 |
| | | Refb | 139·690 | 136·700 | 139·490 | 174·80 | 174·82 | 199·12 | 229·17 | 229·19 |
| 0·5 | − 1·0 | Pre | 164·310 | 164·310 | 168·850 | 175·35 | 209·43 | 211·73 | 238·81 | 238·81 |
| | | Refa | 164·300 | 164·300 | 168·850 | 175·33 | 209·45 | 211·76 | 238·80 | 238·81 |
| | | Refb | 166·720 | 166·730 | 170·040 | 178·47 | 213·66 | 216·16 | 223·57 | 223·57 |
| | − 0·5 | Pre | 121·860 | 136·580 | 159·460 | 165·73 | 180·69 | 205·78 | 227·05 | 228·23 |
| | | Refa | 121·860 | 136·580 | 159·470 | 165·73 | 180·72 | 205·82 | 227·06 | 228·32 |
| | | Refb | 123·600 | 137·380 | 160·610 | 167·80 | 184·72 | 207·40 | 230·93 | 232·03 |
| | 0·0 | Pre | 108·740 | 128·750 | 163·650 | 170·57 | 177·50 | 210·71 | 224·31 | 226·81 |
| | | Refa | 108·740 | 128·770 | 163·670 | 170·58 | 177·54 | 210·77 | 224·46 | 226·84 |
| | | Refb | 110·570 | 129·770 | 164·600 | 127·73 | 181·58 | 211·93 | 228·90 | 230·84 |
| | 0·5 | Pre | 139·490 | 158·030 | 176·510 | 189·99 | 197·70 | 225·24 | 237·33 | 238·88 |
| | | Refa | 139·510 | 158·070 | 176·530 | 190·01 | 197·76 | 225·31 | 237·48 | 238·94 |
| | | Refb | 141·810 | 159·570 | 178·260 | 193·08 | 201·44 | 228·10 | 242·40 | 243·67 |
| | 1·0 | Pre | 192·790 | 192·790 | 204·510 | 218·40 | 218·41 | 260·76 | 260·76 | 262·66 |
| | | Refa | 192·810 | 192·810 | 204·550 | 218·44 | 218·48 | 260·87 | 260·87 | 262·72 |
| | | Refb | 196·630 | 196·630 | 206·600 | 223·87 | 223·88 | 267·82 | 267·83 | 268·64 |

*Note*: Pre: present shell element. Refa: Abaqus [32]. Refb: analytical solution [33].

TABLE 10

*Natural frequencies $\omega_n$ of fully clamped doubly curved shallow shell with elliptical platform*

| $2b/R_y$ | $R_y/R_z$ | | Mode 1 | 2 | 3 | 4 | 5 | 6 | 7 | 8 |
|---|---|---|---|---|---|---|---|---|---|---|
| 0·1 | − 1·0 | Pre | 65·145 | 84·547 | 115·29 | 141·63 | 155·51 | 175·94 | 205·20 | 218·46 |
| | | Refa | 65·090 | 84·355 | 115·02 | 141·29 | 155·17 | 175·09 | 204·88 | 217·31 |
| | | Refb | 65·350 | 84·952 | 116·06 | 142·76 | 156·88 | 177·64 | 207·48 | 220·99 |
| | − 0·5 | Pre | 61·706 | 83·520 | 114·82 | 139·43 | 155·44 | 175·03 | 205·34 | 218·04 |
| | | Refa | 61·646 | 83·328 | 114·54 | 139·08 | 155·10 | 174·18 | 205·03 | 216·89 |
| | | Refb | 61·907 | 83·893 | 115·50 | 140·58 | 156·64 | 176·73 | 207·35 | 220·53 |
| | 0·0 | Pre | 61·711 | 83·721 | 115·02 | 138·86 | 155·63 | 175·01 | 205·52 | 218·14 |
| | | Refa | 61·656 | 83·532 | 114·75 | 138·50 | 155·29 | 174·17 | 205·22 | 217·00 |
| | | Refb | 61·919 | 84·097 | 115·69 | 140·01 | 156·79 | 176·73 | 207·45 | 220·64 |
| | 0·5 | Pre | 65·188 | 85·154 | 115·89 | 139·93 | 156·06 | 175·90 | 205·74 | 218·76 |
| | | Refa | 65·141 | 84·972 | 115·62 | 139·58 | 155·73 | 175·06 | 205·43 | 217·63 |
| | | Refb | 65·402 | 85·560 | 116·61 | 141·10 | 157·31 | 177·65 | 207·80 | 221·32 |
| | 1·0 | Pre | 71·532 | 87·729 | 117·43 | 142·61 | 156·74 | 177·67 | 205·99 | 219·89 |
| | | Refa | 71·498 | 87·554 | 117·17 | 142·27 | 156·41 | 176·84 | 205·68 | 218·77 |
| | | Refb | 71·771 | 88·205 | 118·30 | 143·79 | 158·22 | 179·47 | 208·38 | 222·56 |
| 0·3 | − 1·0 | Pre | 117·430 | 120·410 | 142·98 | 162·55 | 174·49 | 186·50 | 218·50 | 225·86 |
| | | Refa | 117·410 | 120·320 | 142·79 | 162·27 | 174·19 | 185·70 | 218·18 | 224·70 |
| | | Refb | 118·250 | 222·050 | 145·73 | 164·61 | 178·22 | 189·38 | 224·09 | 229·92 |
| | − 0·5 | Pre | 101·410 | 114·710 | 139·32 | 145·32 | 174·47 | 179·22 | 220·12 | 222·37 |
| | | Refa | 101·400 | 114·630 | 139·15 | 144·99 | 174·21 | 178·41 | 219·86 | 221·25 |
| | | Refb | 102·010 | 115·510 | 140·47 | 147·25 | 176·25 | 181·69 | 222·95 | 225·64 |
| | 0·0 | Pre | 101·200 | 116·070 | 140·24 | 140·93 | 176·07 | 179·04 | 221·74 | 223·26 |
| | | Refa | 101·200 | 116·000 | 139·90 | 140·78 | 175·84 | 178·25 | 221·51 | 222·20 |
| | | Refb | 181·820 | 116·780 | 141·86 | 142·30 | 177·45 | 181·63 | 223·86 | 226·60 |
| | 0·5 | Pre | 118·310 | 124·830 | 147·23 | 149·36 | 179·32 | 186·56 | 223·37 | 228·57 |
| | | Refa | 118·320 | 124·780 | 147·11 | 149·06 | 179·11 | 185·83 | 223·15 | 227·57 |
| | | Refb | 119·100 | 125·950 | 148·82 | 151·57 | 181·61 | 189·51 | 226·72 | 232·51 |
| | 1·0 | Pre | 138·260 | 140·970 | 160·97 | 170·15 | 183·89 | 200·36 | 224·92 | 237·40 |
| | | Refa | 138·210 | 140·940 | 160·91 | 169·91 | 183·67 | 199·72 | 224·68 | 236·45 |
| | | Refb | 140·640 | 142·340 | 164·81 | 172·80 | 188·90 | 204·37 | 231·78 | 242·93 |
| 0·5 | − 1·0 | Pre | 166·100 | 170·240 | 188·45 | 194·33 | 203·41 | 203·59 | 238·74 | 240·16 |
| | | Refa | 166·050 | 170·160 | 188·37 | 194·10 | 202·68 | 203·33 | 237·58 | 239·83 |
| | | Refb | 171·660 | 172·900 | 197·86 | 198·77 | 210·10 | 214·54 | 248·13 | 254·21 |
| | − 0·5 | Pre | 149·470 | 155·990 | 157·26 | 176·53 | 186·85 | 205·81 | 230·18 | 245·88 |
| | | Refa | 149·440 | 155·690 | 157·22 | 176·44 | 186·09 | 205·64 | 229·10 | 245·69 |
| | | Refb | 151·310 | 159·610 | 159·64 | 179·44 | 191·08 | 209·49 | 235·36 | 250·96 |
| | 0·0 | Pre | 142·560 | 147·840 | 160·09 | 180·54 | 186·16 | 210·18 | 232·65 | 250·42 |
| | | Refa | 142·240 | 147·810 | 160·07 | 180·49 | 185·46 | 210·08 | 231·71 | 250·30 |
| | | Refb | 146·430 | 149·690 | 161·90 | 182·45 | 190·61 | 212·42 | 237·87 | 253·30 |
| | 0·5 | Pre | 165·520 | 176·390 | 176·58 | 193·95 | 204·93 | 216·85 | 246·05 | 253·66 |
| | | Refa | 165·290 | 176·340 | 176·58 | 193·94 | 204·36 | 216·77 | 245·23 | 253·54 |
| | | Refb | 170·020 | 178·830 | 179·93 | 198·27 | 210·79 | 222·04 | 253·33 | 260·25 |
| | 1·0 | Pre | 197·740 | 198·940 | 211·68 | 223·99 | 229·05 | 235·35 | 255·83 | 265·15 |
| | | Refa | 197·740 | 198·910 | 211·53 | 223·91 | 229·03 | 234·90 | 255·65 | 264·43 |
| | | Refb | 205·170 | 205·510 | 218·85 | 239·10 | 239·66 | 246·36 | 274·52 | 279·01 |

*Note*: Pre: present shell element. Refa: Abaqus [32]. Refb: analytical solution [33].

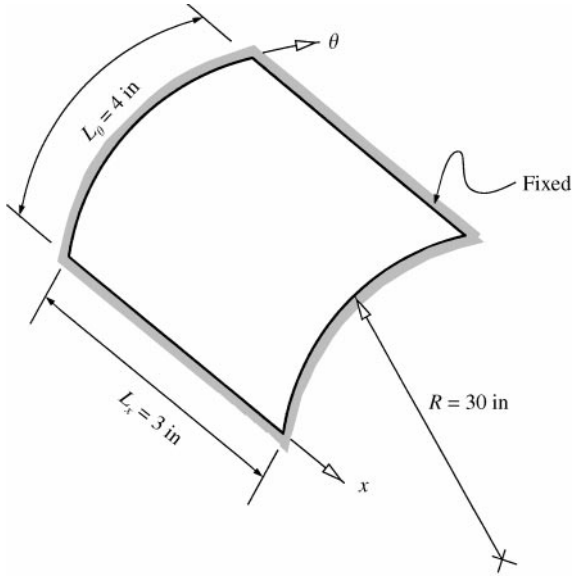


Figure 9. A clamped cylindrical shell panel.

TABLE 11

*The Natural frequencies $\omega_n$ of clamped cylindrical panel*

| $n$ | Expt | Refa | Refb | Refc | LAG9 | ASL9 | Present |
|---|---|---|---|---|---|---|---|
| 1 | 814 | 869·560 | 890 | 870 | 897·142 | 879·244 | 878·253 |
| 2 | 940 | 957·560 | 973 | 958 | 989·541 | 968·427 | 966·972 |
| 3 | 1260 | 1287·560 | 1311 | 1288 | 1356·33 | 1302·47 | 1300·51 |
| 4 | 1306 | 1363·210 | 1371 | 1364 | 1407·25 | 1378·65 | 1377·21 |
| 5 | 1452 | 1440·260 | 1454 | 1440 | 1494·90 | 1455·03 | 1453·50 |
| 6 | 1802 | 1755·590 | 1775 | 1753 | 1854·01 | 1770·87 | 1768·54 |
| 7 | 1735 | 1779·630 | 1816 | 1779 | 1996·44 | 1802·15 | 1797·46 |
| — | 1770 | — | — | — | — | — | — |
| 8 | 2100 | 2056·080 | 2068 | 2055 | 2197·01 | 2079·55 | 2077·21 |
| 9 | 2225 | 2221·750 | 2234 | 2218 | 2368·94 | 2242·47 | 2239·54 |
| 10 | 2280 | 2295·310 | 2319 | 2288 | 2505·70 | 2313·59 | 2306·38 |
| 11 | 2518 | 2553·120 | — | | 2742·38 | 2582·36 | 2573·77 |
| 12 | 2622 | 2569·500 | — | | 3002·53 | 2594·85 | 2581·58 |
| 13 | 3016 | 3041·690 | — | | 3365·68 | 3069·81 | 3048·21 |
| 14 | 3188 | 3081·280 | — | | 3440·05 | 3119·12 | 3107·57 |
| 15 | 3113 | 3112·900 | — | | 3466·82 | 3121·52 | 3111·13 |
| 16 | 3332 | 3299·670 | — | | 3646·96 | 3321·82 | 3311·50 |
| — | 3348 | | — | | | | |
| 17 | 3403 | 3485·700 | — | | 4028·54 | 3564·75 | 3517·92 |
| — | 3445 | | — | | | | |
| 18 | 3699 | 3686·580 | — | | 4277·26 | 3684·92 | 3668·25 |
| 19 | 3812 | 3855·450 | — | | 4303·11 | 3857·51 | 3823·05 |
| 20 | 3930 | 3980·780 | — | | 4625·68 | 4027·97 | 3970·34 |

*Note*: Expt: experiments results [34]. Refa: numerical solution [37]. Refb: numerical solution [35]. Refc: analytical solution [36]. LAG9: nine-node shell element [17]. ASL9: assumed strain shell element [19].

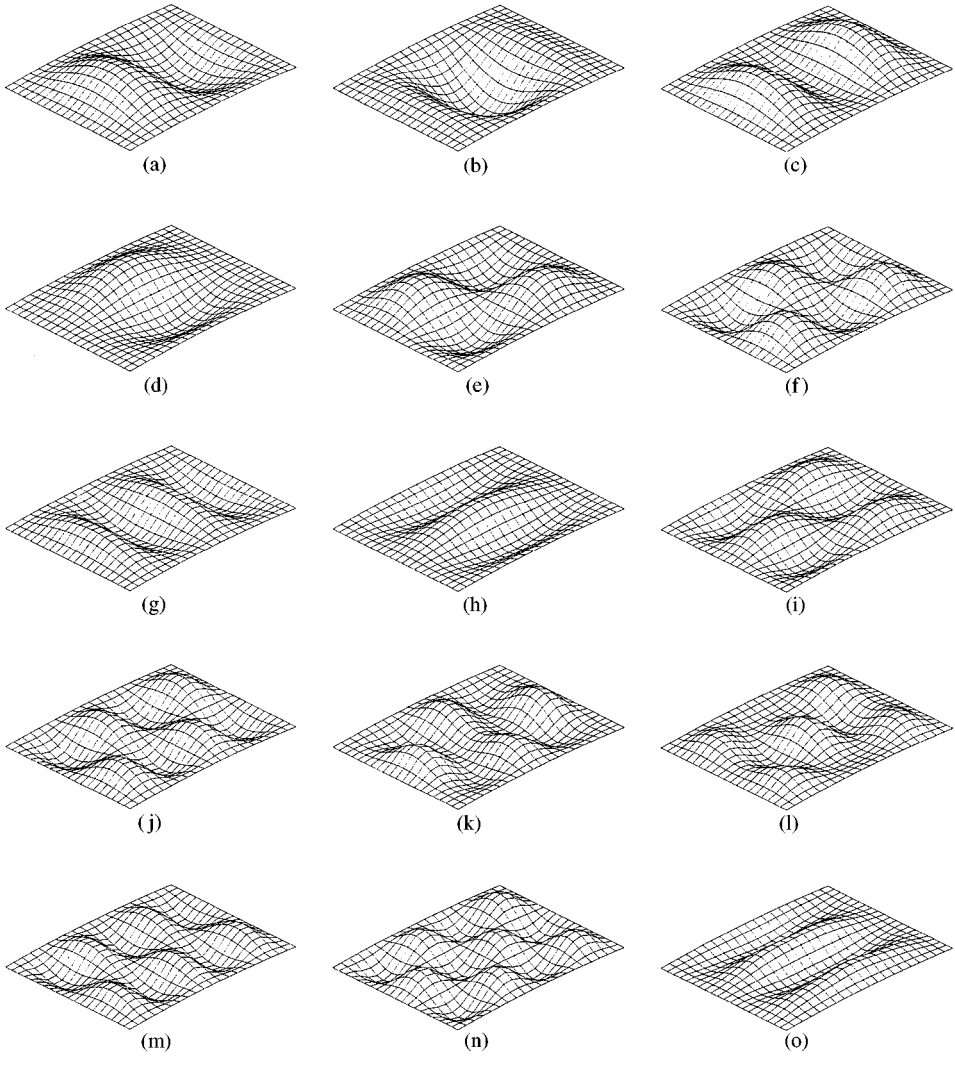


Figure 10. Mode shapes of a clamped cylindrical panel: (a) mode 1–(o) mode 15.

TABLE 12

*Natural frequencies $\omega_n$ of a curved fan blade with two aspect ratios*

| Mode | for $a/b = 1$ | | | | | For $a/b = 5$ | | | |
|---|---|---|---|---|---|---|---|---|---|
| $n$ | Refa | Refb | LAG9 | ASL9 | Present | Refa | LAG9 | ASL9 | Present |
| 1 | 10·515 | 10·589 | 10·623 | 10·605 | 10·604 | 4·3223 | 4·4416 | 4·4409 | 4·4369 |
| 2 | 16·990 | 16·981 | 17·199 | 17·176 | 17·172 | 7·1753 | 8·4678 | 7·1220 | 7·1174 |
| 3 | 30·649 | 30·641 | 30·473 | 30·310 | 30·315 | 22·8990 | 23·2100 | 22·7970 | 22·7740 |
| 4 | 42·229 | 42·211 | 42·314 | 42·355 | 42·356 | 25·9950 | 26·6930 | 26·6750 | 26·6440 |
| 5 | 47·684 | 47·668 | 47·385 | 47·440 | 47·438 | 42·3940 | 42·6290 | 42·4090 | 42·3400 |
| 6 | 65·450 | 65·439 | 64·439 | 63·957 | 63·957 | 65·2170 | 65·9230 | 65·9330 | 65·8950 |
| 7 | 89·991 | 89·727 | 89·524 | 89·578 | 89·577 | 65·2810 | 66·7340 | 66·5700 | 66·4780 |
| 8 | 90·143 | 89·947 | 89·920 | 90·007 | 90·009 | 67·0640 | 67·6690 | 67·4150 | 67·2090 |

*Note*: Refa: theoretical solution [38]. Refb: theoretical solution [39]. LAG9: nine-node shell element [17]. ASL9: assumed strain shell element [19].

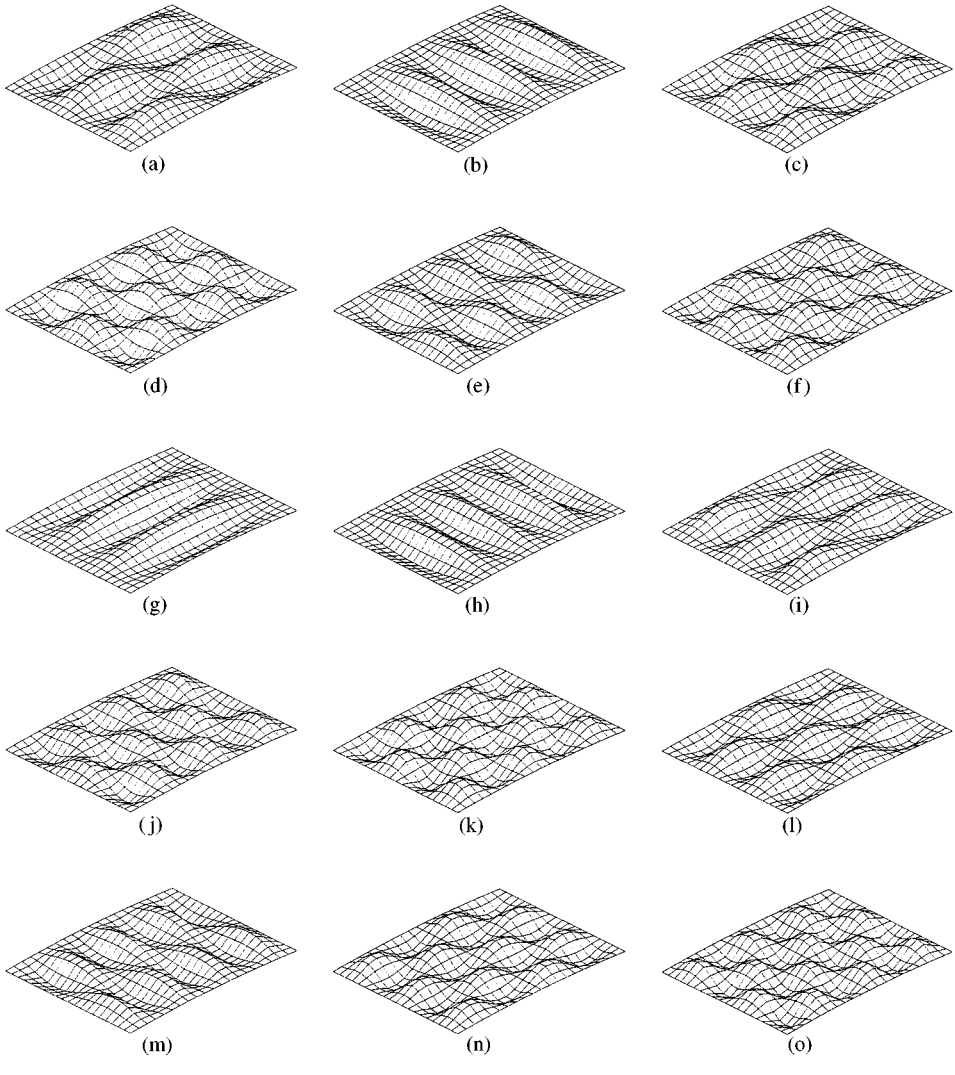


Figure 11. Mode shapes of a clamped cylindrical panel: (a) mode 16–(o) mode 30.

## ACKNOWLEDGMENT

The first author is grateful to the late Professor E. Hinton for his encouragement throughout this work in Swansea.

## REFERENCES

1. A. E. H. Love 1888 *Philosophical Transactions of the Royal Society* **179**, 527–546. The small vibrations and deformations of thin elastic shell.
2. L. H. Donell 1933 *NASA Report* 479. Stability of thin-walled tubes under torsion.
3. A. W. Leissa 1973 *NASA PA*-288, *Washington, DC*. Vibrations of shells.
4. M. S. Qatu 1992 *Shock Vibration Digest* **24**, 3–15. Review of shallow shell vibration research.

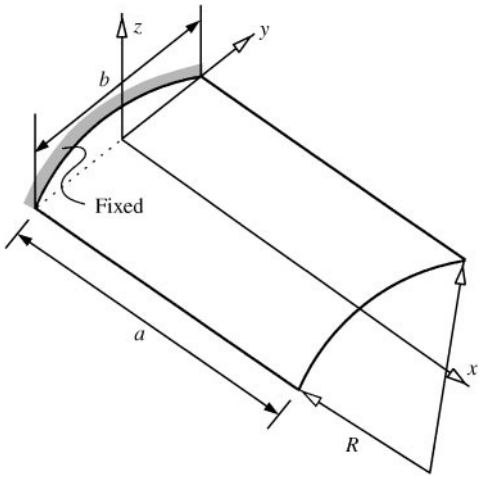


Figure 12. Geometry of curved fan blade.

5. K. M. LIEW, C. W. LIM and S. KITIPORNCHAI 1997 *Applied Mechanics Reviews* **50**, 431–444. Vibration of shallow shells: a review with bibliography.
6. A. ADINI 1961 *Ph.D Dissertation*, *University of California*, *Berkeley*, Analysis of shell structures by the finite element methods.
7. R. H. GALLAGHER 1975 *Proceedings of the World of the conference on Finite element methods in structural mechanics*, *Bournemouth*. Shell elements.
8. S. AHMAD, B. M. IRONS and O. C. ZIENKIEWICZ 1970 *International Journal of Numerical Methods in Engineering* **2**, 419–451. Analysis of thick and thin shell structures by curved finite elements.
9. W. P. DOHERTY, E. J. WILSON and R. L. TAYLOR 1969 *UC-SESM Report No*. 69-3, *Department of Civil Engineering*, *University of California*, *Berkeley*. Stress analysis of axisymmetric solids utilizing higher order quadrilateral finite element.
10. O. C. ZIENKIEWICZ, R. L. TAYLOR and J. M. TOO 1971 *International Journal of Numerical Methods in Engineering* **3**, 275–290. Reduced integration technique in general analysis of plates and shells.
11. K. J. BATHE and E. N. DVORKIN 1985 *International Journal of Numerical Methods in Engineering* (*Short Communication*) **21**, 367–383. A four-node plate bending element based on Mindlin–Reissner plate theory and a mixed formulation.
12. T. BELYTSCHKO, B. L. WONG and H. STOLARSKI 1989 *International Journal of Numerical Methods in Engineering* **28**, 385–414. Assumed strain stabilization procedure for the 9-node Lagrangian shell element.
13. K. M. LIEW 1995 *Journal of Sound and Vibration* **180**, 163–176. Research on thick plate vibration: a literature survey.
14. T. J. R. HUGHES 1987 *The Finite Element Method—Linear Static and Dynamic Finite Element Analysis*. Englewood Cliffs, NJ: Prentice-Hall.
15. K. J. BATHE 1982 *Finite Element Procedures in Engineering Analysis*. Englewood Cliffs NJ: Prentice-Hall.
16. O. C. ZIENKIEWICZ and R. L. TAYLOR 1989 *The Finite Element Method*, Vol. 1. London: McGraw-Hill; fourth edition.
17. W. KANOK-NUKULCHAI 1979 *International Journal of Numerical Methods in Engineering* **14**, 179–200. A simple and efficient finite element for general shell analysis.
18. S. J. LEE and W. KANOK-NUKULCHAI 1998 *International Journal of Numerical Methods in Engineering* **4**, 777–798. A nine-node assumed strain finite element for large-deformation analysis of laminated shells.
19. H. C. HUANG and E. HINTON 1986 *International Journal of Numerical Methods in Engineering* **22**, 73–92. A new nine-node degenerated shell element with enhanced membrane and shear interpolation.

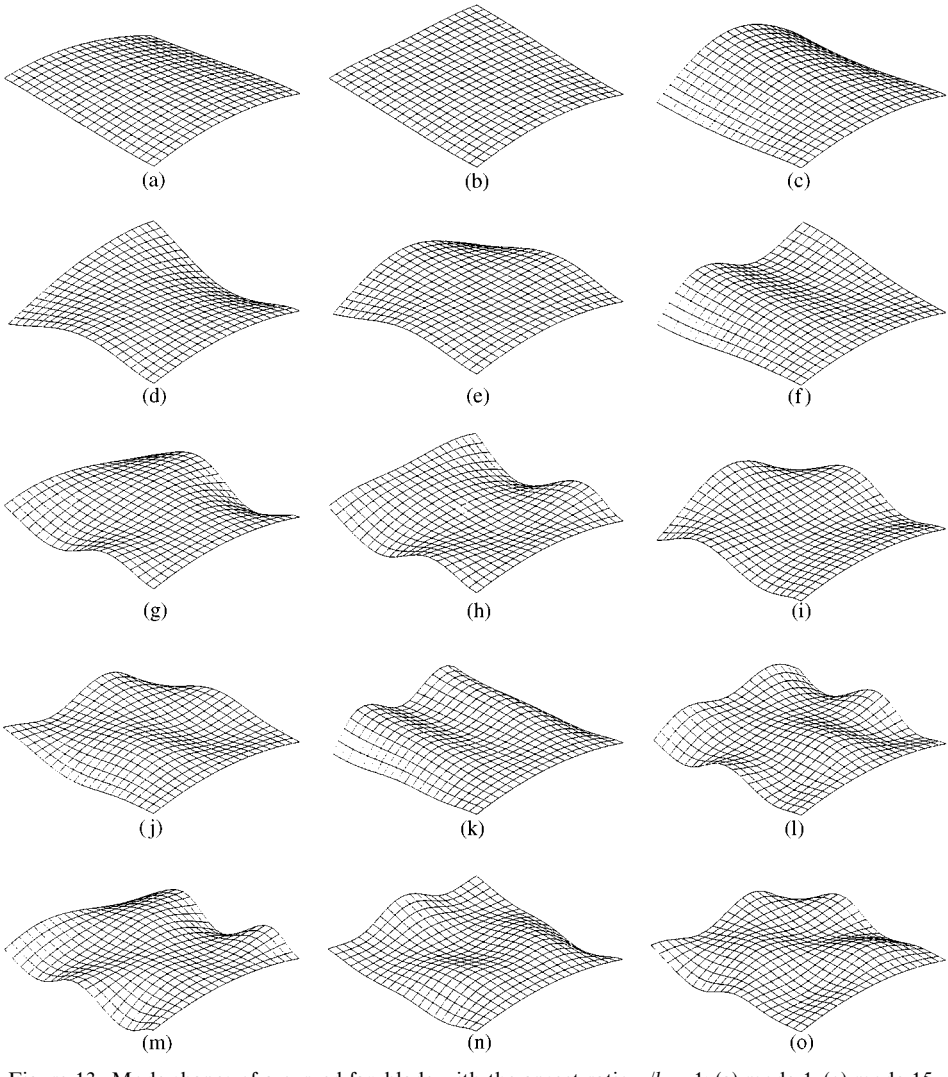


Figure 13. Mode shapes of a curved fan blade with the apsect ratio $a/b = 1$: (a) mode 1–(o) mode 15.

20. S. J. LEE and Y. B. KIM 1994 *Journal of the Architectural Institute of Korea* **10**, 181–188. Finite element analysis of laminated plates with assumed strain method.
21. A. W. LEISSA 1973 *Journal of Sound and Vibration* **31**, 257–293. The free vibration of rectangular plates.
22. B. S. AI. JANABI and E. HINTON 1988 in *Numerical Methods and Software for Dynamic Analysis of Plates and Shells* (E. Hinton, editor) 167–204. Swansea: Pineridge Press. A study of the free vibrations of square plates with various edge conditions.
23. S. SRINIVAS, C. V. JOGA RAO and A. K. RAO 1970 *Journal of Sound and Vibration* **12**, 187–199. An exact analysis for vibration of simply supported homogeneous and laminated, thick rectangular plates.
24. J. N. REDDY and N. D. PHAN 1985 *Journal of Sound and Vibration* **98**, 157–170. Stability and vibration of isotropic and laminated plates according to a higher-order shear deformation theory.
25. E. HINTON and DJ. VUKSANOVIC 1988 in *Numerical Methods and Software for Dynamic Analysis of Plates and Shells* (E. Hinton, editor) 1–47. Swansea: Pineridge Press. Closed form solutions for dynamic analysis of simply supported Mindlin plates.

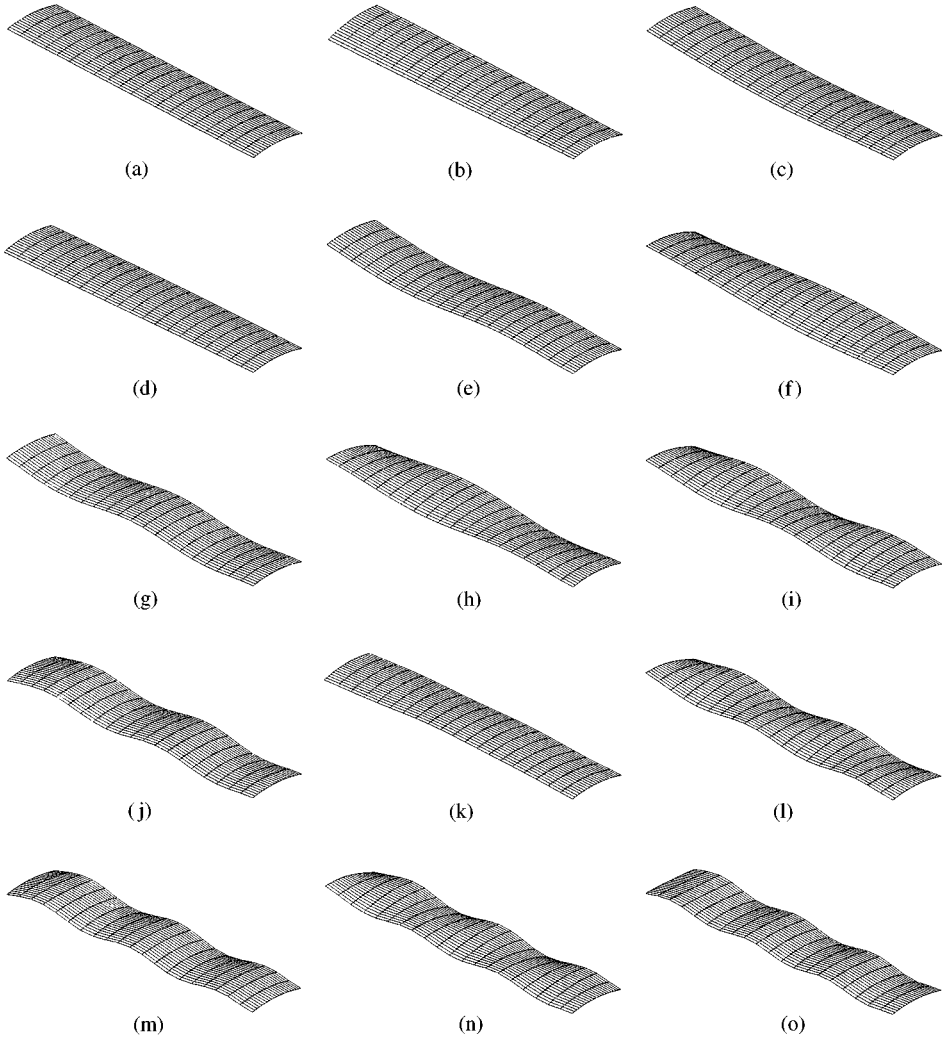


Figure 14. Mode shapes of a curved fan blade with the aspect ratio: $a/b = 5$: (a) mode 1–(o) mode 15.

26. E. REISSNER 1945 *ASME Journal of Applied Mechanics* **12**, 69–76. The effect of transverse shear deformation on the bending of elastic plate.
27. D. J. DAWE and O. L. ROUFAEIL 1980 *Journal of Sound and Vibration* **69**, 345–359. Rayleigh–Ritz vibration analysis of Mindlin plates.
28. D. J. DAWE 1978 *Journal of Sound and Vibration* **59**, 441–452. Finite strip models for vibration of Mindlin plates.
29. E. HINTON, DJ. VUKSANOVIC and H. C. HUANG 1988 in *Numerical Methods and Software for Dynamic Analysis of Plates and Shells* (E. Hinton, editor) 93–166. Swansea: Pineridge Press. Finite element free vibration and bucking analysis of initially stesses Mindlin plates.
30. A. W. LEISSA 1969 *NASA SP*-160, *Washington*, *DC*. Vibration of plates.
31. K. M. LIEW 1992 *Journal of Sound and Vibration* **154**, 261–269. Use of two-dimensional orthogonal polynomials for vibration analysis of curcular and elliptical plates.
32. *ABAQUS Theory and User Manuals*. Hibbit, Karlson and Sorensen, Inc., Version 5.7.
33. K. M. LIEW 1995 *Journal of Engineering Mechanics* **121**, 1277–1283. Vibration behaviour of doubly curved shallow shells of curvilinear planform.

34. J. M. DEB NATH 1969 *Ph.D. Thesis, University of Southampton*. Dynamics of rectangular curved plates.
35. M. PETYT 1971 *Journal of Sound and Vibration* **15**, 381–395. Vibration of curved plates.
36. C. W. LIM and K. M. LIEW 1995 *International Journal of Mechanical Sciences* **37**, 277–295. A higher order theory for vibration of shear deformable cylindrical shallow shells.
37. M. D. OLSON 1971 *Journal of Sound and Vibration* **3**, 299–318. Dynamic analysis of shallow shells with a doubly-curved triangular finite element.
38. J. K. LEE, A. W. LEISSA and A. J. WANG 1981 *Journal of Sound and Vibration* **78**, 311–328. Vibrations of cantilevered shallow cylindrical shells of rectangular planform.
39. C. W. LIM and K. M. LIEW 1994 *Journal of Sound and Vibration* **173**, 343–375. A ph-z Ritz formulation for flexural vibration of shallow cylindrical shell of rectangular planform.